DEVELOPING ECO-ADAPTIVE CRUISE CONTROL SYSTEMS

Final Report

TranLIVE

Hesham Rakha and Kyoungho Ahn

January 2014

DISCLAIMER

The contents of this report reflect the views of the authors, who are responsible for the facts and the accuracy of the information presented herein. This document is disseminated under the sponsorship of the Department of Transportation, University Transportation Centers Program, in the interest of information exchange. The U.S. Government assumes no liability for the contents or use thereof.

1. Report No.	2. Government Accession No.	3. Recipient's Catalog No.
4. Title and Subtitle Developing Eco-adaptive Cruise Control Systems		5. Report Date January 2014
		6. Performing Organization Code KLK900-SB-002
7. Author(s) Hesham Rakha and Kyoungho Ahn		8. Performing Organization Report No. N14-06
9. Performing Organization Name and Address Virginia Polytechnic Institute & State University 1880 Pratt Dr, Suite 2006 Blacksburg, VA 24060 Source Organization Name and Address NIATT & TranLIVE University of Idaho 875 Perimeter Dr. MS0901 Moscow, ID 83844-0901		10. Work Unit No. (TRAIS) 11. Contract or Grant No. DTRT12-G-UTC17
12. Sponsoring Agency Name and Address US Department of Transportation Research and Special Programs Administration 400 7th Street SW Washington, DC 20509-0001		13. Type of Report and Period Covered Final Report: 1/1/2012 – 12/31/2013 14. Sponsoring Agency Code USDOT/RSPA/DIR-1
15. Supplementary Notes:		

16. Abstract

The study demonstrates the feasibility of two eco-driving applications which reduces vehicle fuel consumption and greenhouse gas emissions. In particular, the study develops an eco-drive system that combines eco-cruise control logic with state-of-the-art car-following models and evaluates Eco-Lanes and SPD-HARM applications. The research investigated the potential of developing an eco-drive system that combines an Eco-Cruise Control (ECC) system with state-of-the-art car-following models. The system makes use of topographic information, the spacing between the subject and lead vehicle, and a desired (or target) vehicle speed and distance headway as input variables. The study demonstrated that the proposed system can significantly improve fuel efficiency while maintaining reasonable vehicle spacing. Furthermore, the study also demonstrated that a dynamic car-following spacing threshold significantly reduces the average vehicle spacing compared to a fixed car-following spacing threshold. The study finally demonstrated that non-ECC-equipped vehicles can significantly reduce their own fuel consumption just by following a lead ECC-equipped vehicle. Further, the research investigated the feasibility of Eco-Lanes applications that attempt to reduce system-wide fuel consumption and GHG emission levels through lane management strategies. The study demonstrated that the proposed Eco-Lanes system can significantly improve fuel efficiency and air quality while reducing average vehicle travel time and total system delay. The study also found that the optimum throttle levels and the optimum eco-speed limits can significantly improve the mobility and fuel economy.

17. Key Words Eco-driving, Eco-cruise control, Car-following, Eco-Lanes, Connected Vehicles	18. Distribution Statement Unrestricted; Document is available to the public through the National Technical Information Service; Springfield, VT.

19. Security Classif. (of this report) Unclassified	20. Security Classif. (of this page) Unclassified	21. No. of Pages 38	22. Price …

Form DOT F 1700.7 (8-72) Reproduction of completed page authorized

TABLE OF CONTENTS

EXECUTIVE SUMMARY

The study demonstrates the feasibility of two eco-driving applications which reduces vehicle fuel consumption and greenhouse gas emissions. The study develops an eco-drive system and Eco-Lanes applications. In particular, the study develops an eco-drive system that combines eco-cruise control logic with state-of-the-art car-following models and evaluates Eco-Lanes and SPD-HARM applications.

The research investigated the potential of developing an eco-drive system that combines an ECC system with state-of-the-art car-following models. The system makes use of topographic information, the spacing between the subject and lead vehicle, and a desired (or target) vehicle speed and distance headway as input variables. The study demonstrated that the proposed system can significantly improve fuel efficiency while maintaining reasonable vehicle spacing. One of the test vehicles, a 2011 Toyota Camry, saved 27 percent in fuel consumption with an average spacing of 47 m along the I-81 study section. The study found that the car-following threshold setting significantly affects the fuel economy and the spacing between vehicles. Furthermore, the study also demonstrated that a dynamic car-following spacing threshold significantly reduces the average vehicle spacing compared to a fixed car-following spacing threshold. The study also evaluated the impacts of variable vehicle power and found that vehicle operations at lower power demands significantly enhance vehicle fuel economy (up to 49 percent). The study finally demonstrated that non-ECC-equipped vehicles can significantly reduce their own fuel consumption just by following a lead ECC-equipped vehicle.

Further, the research investigated the feasibility of Eco-Lanes applications that attempt to reduce system-wide fuel consumption and GHG emission levels through lane management strategies. The study focused its efforts on evaluating various Eco-Lanes and SPD-HARM applications using the INTEGRATION microscopic traffic simulation software. The study demonstrated that the proposed Eco-Lanes system can significantly improve fuel efficiency and air quality while reducing average vehicle travel time and total system delay. For this case study, the proposed system reduced travel time, delay, fuel consumption, HC, CO, and CO2 emissions by 8.5%, 23%, 4.5%, 3.1%, 3.4%, and 4.6%, respectively, compared with the base case scenario. The study also examined the feasibility of a predictive Eco-Lanes system. This system predicts the onset of congestion and starts the Eco-Lanes system before congestion occurs. The simulation study found that the 30-minute predictive Eco-Lanes system produced greater reductions in fuel consumption and CO2 emissions compared with the non-predictive Eco-Lanes system. The study also found that the optimum throttle levels and the optimum eco-speed limits can significantly improve the mobility, energy savings, and air quality of such systems. Furthermore, the study demonstrated that SPD-HARM as an Eco-Lanes application produced reductions in delay, fuel consumption, HC, CO, NOx, and CO2 emissions by 7.6%, 6.3%, 23.9%, 26.1%, 17.2%, and 4.4%, respectively, compared with the base case scenario.

Future research should quantify the potential benefits of using the proposed Eco-Lanes systems on different networks with various vehicle types. Also, further studies are required to characterize the optimum eco-lanes specifications, such as the spatial and temporal eco-lanes boundaries, and to enhance the optimum eco-speed limit algorithms. Furthermore, the car-following behavior of non-eco-vehicles should be investigated. Finally, further research is needed to validate the simulation outputs using field tests.

The research resulted in the following peer-reviewed publications:

1. Saerens B., Rakha H., and Van den Bulck E. (2012), "Assessment of Eco-Cruise Control Calculation Methods," Transportation Research Board 91st Annual Meeting, Washington DC, January 22-26, CD-ROM [Paper # 12-4698].
2. Ahn K., Rakha H., and Park S. (2013), ECO-Drive Application: Algorithmic Development and Preliminary Testing, Transportation Research Record, No.2341, Air Quality 2013, Vol.2, pp. 1–11. DOI: 10.3141/2341-01
3. Park S., Rakha H., Ahn K., and Moran K. (2013), "Fuel Economy Impacts of Manual, Conventional Cruise Control, and Predictive Eco-Cruise Control Driving," *International Journal of Transportation Science and Technology*, Vol. 2, no. 3, pp. 227-242.
4. Saerens B., Rakha H., Diehl M., Van den Bulck E. (2013), "Eco-Cruise Control for Passenger Vehicles: Methodology," *Transportation Research Part D: Transport and Environment*, Vol. 19, pp. 20-27.
5. Ahn K. and Rakha H. (2014), "Eco-Lanes Applications: Preliminary Testing and Evaluation" Transportation Research Board 93rd Annual Meeting, Washington D.C., [Paper 14-3784].

PROBLEM OVERVIEW

The proposed study demonstrates the feasibility of two eco-driving applications that enhances a vehicle's fuel economy and reduces greenhouse gas emissions. In particular, the study focuses its efforts on developing an eco-drive system and investigating the feasibility of Eco-Lanes applications. The study develops an eco-drive system that combines eco-cruise control logic with state-of-the-art car-following models. Further, the study focuses its efforts on evaluating Eco-Lanes and SPD-HARM applications.

There are several variables that affect vehicle fuel consumption levels. Roadway grade is one of the major variables that affect vehicle fuel consumption levels. On upgrade sections, vehicles utilize additional power to overcome the grade resistance, thus consuming more fuel than under normal conditions [1]. Studies have shown that a roadway grade results in significant increases in vehicle fuel consumption and emission levels [2, 3]. Park and Rakha demonstrated that a 6 percent increase in a roadway grade could increase vehicle fuel consumption levels in the range of 40 to 94 percent, and a 1 percent grade could result in 13 to 18 percent increases in fuel consumption levels [3]. A recent study concluded that the overall fuel economy along a flat route was superior to that on a hilly route by approximately 15 to 20 percent [4]. Thus energy-efficient operations on hilly roads could produce significant savings in fuel consumption levels.

A study has investigated the potential for developing eco-cruise control systems that will allow vehicles to travel within a desired speed range as opposed to driving at a single desired speed regardless of the fuel economy implications [5]. The system utilizes the gravitational force to allow vehicles to travel at higher speeds (within the upper bound of the desired speed) while traveling downhill and travel at lower speeds (within the lower bound of the desired speed) while traveling along upgrade sections. The key input variables to the eco-cruise control system are the desired speed and a speed range. In addition, the system requires a high resolution digital map and a GPS system to identify the vehicle location. The speed range identifies the maximum and minimum speed the driver is willing to accept. Using the driver input the system maintains the desired speed on flat roadways. Once a vehicle encounters an uphill road section, the eco-cruise control system lowers the target speed to reduce the engine load and reduce the fuel consumption level. On the other hand, when the vehicle travels along a downhill section, the system increases the target speed within the desired speed range. This mechanism allows the vehicle to use the force of gravity to its advantage. The results are very promising and indicate potential savings of up to 10 percent in fuel economy depending on the input speed range as demonstrated by the results along a 26-mile section of I-81 between Roanoke and Blacksburg, Virginia.

Another study also developed an eco-predictive cruise control system that utilizes topographical data to develop proactive vehicle control strategies that minimize the vehicle's fuel consumption level [6]. The system entails eco-cruise control system logic through the use of a moving horizon dynamic programming algorithm with powertrain and fuel consumption models to determine the optimum throttle level, speed, and gear shift points with the objective of minimizing the vehicle's fuel consumption level.

The Eco-Lanes concept integrates dedicated highway lanes that are optimized to reduce fuel consumption and improve air quality. In the Eco-Lanes drivers are required to operate the vehicle with recommended and/or variable speeds to reduce transportation energy consumption and improve vehicle mobility. The proposed system fits within the Eco-Lane concept, a concept within the

Applications for the Environment: Real-time Information Synthesis (AERIS) Program, that was initiated by the U.S. Department of Transportation [7]. In the Eco-Lanes drivers are required to operate the vehicle with recommended and/or variable speeds to reduce transportation energy consumption and improve vehicle mobility.

Few studies have been performed regarding the Eco-Lanes applications. The Applications for the Environment: Real-time Information Synthesis (AERIS) Program was initiated by the U.S. Department of Transportation [7-10] in 2011. The Eco-Lanes was introduced as one of six AERIS Transformative Concepts. The AERIS program is also considered as one of Connected Vehicle Environmental Applications since many applications in the AERIS program are operated with the vehicle-to-vehicle (V2V) and vehicle-to-infrastructure (V2I) communications to improve fuel efficiency and air quality.

The Eco-Lanes concept includes the following applications: Eco-Lanes, Eco-Speed Harmonization (SPD-HARM), Eco-Ramp Metering, Eco-Cooperative Adaptive Cruise Control (CACC), Multi-modal Traveler Information, and Connected Eco-Driving. Among the Eco-Lanes applications, the Eco-SPD-HARM and Eco-CACC applications are fundamentally identical to the SPD-HARM and CACC applications of connected vehicle programs. Major innovative research efforts related to CACC and SPD-HARM development have been performed in recent years in the United States, Europe, and various Asian countries.

One of the major accomplishments in CACC research is the SARTRE project (SAfe Road Trains for the Environment), which is the most recent European Commission co-funded project that was completed in 2012 [11-13]. The SARTRE effort developed strategies and technologies to allow vehicle platoons to operate on public highways producing significant environmental, safety and comfort benefits. Another notable CACC program was showcased at Eindhoven, the Netherlands in May, 2011 aiming at longer term implementation of a high market penetration for cooperative vehicles. The field tests showed that the practical results matched the theoretical analysis demonstrating the possibilities for vehicle following headways of 0.7 s for a test fleet of six passenger cars [11-13]. In the United States, the University of California Partners for Advanced Transit and Highways (PATH) Program implemented a CACC system on two Infiniti FX-45 test vehicles that were equipped with a data acquisition system [14-17]. Regarding energy saving and emission reduction, the SARTRE study claimed that one of the major benefits of CACC was reducing aerodynamic drag that leads to better fuel efficiency and less GHG emissions [6]. Aerodynamic drag reduction or aerodynamic coefficient is achieved through short following distances of platooning vehicles. The PATH study also claimed that vehicle platooning could significantly reduce fuel consumption levels [14-17].

SPD-HARM has been implemented by reducing speed variability among vehicles. Previous studies indicate that the strategy has been reasonably successful in achieving its objectives. For example, a case study in Dutch found that speed harmonization promotes stable traffic flow and reliable travel times and reduces traffic congestions, which result in significant air quality benefits [18-20]. A number of algorithms of SPD-HARM have been developed to recommend the target speed of SPD-HARM or the Variable Speed Limit (VSL) algorithms. Some of them are simple algorithms. Some other algorithms are more complicated using fuzzy logic or regression models [21-26]. However, few studies are investigated to evaluate both the mobility and environmental benefits of SPD-HARM. This

study investigates the feasibility of SPD-HARM applications that can enhance vehicle mobility, fuel efficiency, and air quality.

The objective of this study is two-fold. First, the study integrates the predictive eco-cruise control system with car-following models to develop an eco-drive system that reverts between car-following and eco-cruise control logic depending on the vehicle spacing. The study also quantifies the fuel savings associated with the proposed eco-drive application. The proposed study focuses its efforts on integrating predictive cruise control, optimum vehicle acceleration and deceleration controllers within car-following models. The potential benefits of such a system are significant since the transportation sector is responsible for nearly two-thirds of the total gasoline consumption in the United States (U.S.). The feasibility of the proposed system is evaluated using computer simulations. As CO_2 emissions are directly associated with fuel use, the results presented in this study are also applicable to vehicle tailpipe CO_2 emissions. Second, the study evaluates Eco-Lanes applications using a microscopic simulation model and quantifies the mobility benefits and the reduction of fuel consumption and emissions. In particular, various Eco-Lanes systems and SPD-HARM application are tested and evaluated in this study.

PROPOSED ECO-DRIVE APPLICATION

The research team developed a predictive Eco-Cruise Control (ECC) system that generates optimal vehicle controls in response to changes in roadway grades. The proposed eco-drive system employs the operational concept of this predictive ECC system. The system optimizes the vehicle controls in advance using a widely used dynamic programming (DP) implementation of Dijkstra's shortest path algorithm. The Virginia Tech Comprehensive Power-based Fuel Consumption Model (VT-CPFM) is used in this study because of its simplicity, accuracy, and ease of calibration. A detailed description of the fuel consumption model and the validation of the model are described elsewhere [27].

There are three system parameters used, namely: the stage length (d_s), the look-ahead distance (d_o), and the optimization implementation distance (d_f), as illustrated in Figure 1. The stage length (d_f), the first parameter, is the unit of discretization for solving the problem. In other words, the estimated vehicle optimal speed remains constant for the duration of a stage. The look-ahead distance (d_o), the second parameter, is the distance for which the optimization is performed. Finally, the optimization implementation distance (d_f), the last parameter, is the distance for which the optimized plan is implemented. The detailed description is found in an earlier publication [6].

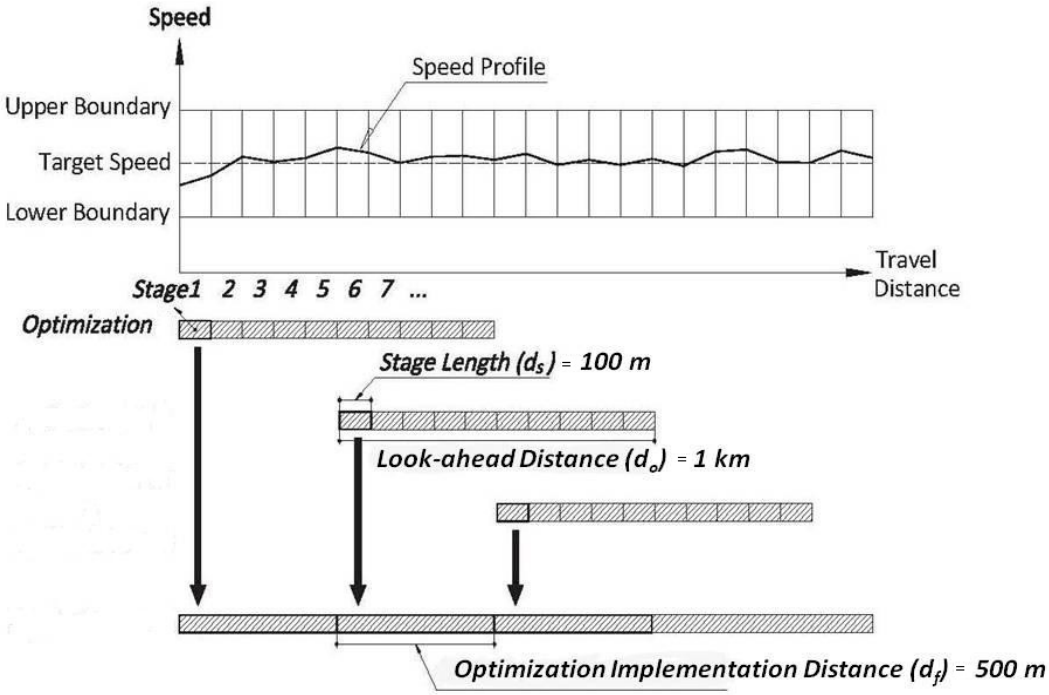

FIGURE 1 Proposed Optimization Methods

For example, assume that a driver plans a 5-km long trip and defines the stage length (d_s), the look-ahead distance, and the optimization implementation distance (d_f) as 100 m, 1 km, and 500 m, respectively. First, the system calculates the optimal vehicle speed for a look-ahead distance, 1 km section, from 0 m to 1000 m. Since the stage length (d_s) is 100 m, the optimal speed is estimated for every 100 m section. The estimated vehicle optimal speed remains constant for 100 m. Since the optimization implementation distance (d_f) is 500 m, when vehicle arrives at 500m the system repeats the optimization looking ahead from 500 m to 1500 m. Then the optimization is carried out every 500 m using the road profile over the next 1 km section.

In order to maintain and adjust the vehicle speed, a vehicle powertrain model is integrated with the eco-cruise control system to model the instantaneous power and other powertrain characteristics. The powertrain model also includes a gear shifting model. The engine speed and torque are then used to compute the vehicle power using a parabolic vehicle engine model that was developed by Ni and Henclewood [28]. A more detailed description of the powertrain model is provided in the literature [29].

Proposed car-following Algorithm

Car-following models assume that there is a relationship between the distance to the preceding vehicle and the speed of the following vehicle when the inter-vehicle spacing is sufficiently small. The process of car-following is modeled as equations of motion under steady-state conditions plus a number of constraints that govern the behavior of vehicles while moving from one steady-state to another (decelerating and accelerating).

Steady-State Modeling

This study will consider the use of the Van Aerde steady-state car-following model which is a nonlinear single-regime functional form. The model was proposed in Van Aerde [30] and Van Aerde and Rakha [31, 32].

$$s_n(t) = c_1 + c_3 u_n(t + \Delta t) + \frac{c_2}{u_f - u_n(t + \Delta t)} \quad (1)$$

where $s_n(t)$ is vehicle spacing at time t, $u_n(t)$ is speed of vehicle n at time t (km/h), u_f is free-flow speed (km/h), Δt is length of time interval, c_1 is fixed distance headway constant (km), c_2 is first variable headway constant (km^2/h), and c_3 is second variable distance headway constant (h).

Rakha [33] demonstrated that the c_1, c_2, and c_3 parameters can be computed as shown in Equation (2). In order to ensure that the speed estimates are realistic the model parameters must satisfy the condition of Equation (3) [33].

$$c_1 = \frac{u_f}{k_j u_c^2}\left(2u_c - u_f\right); c_2 = \frac{u_f}{k_j u_c^2}\left(u_f - u_c\right)^2; c_3 = \left(\frac{1}{q_c} - \frac{u_f}{k_j u_c^2}\right) \quad (2)$$

$$q_c \le \frac{k_j u_c u_f}{2u_f - u_c} \quad (3)$$

where u_c is speed-at-capacity (km/h), k_j is jam density (veh/km), and q_c is the capacity (veh/h).

Typically the vehicle speed or the acceleration level is considered as the control variable. Consequently, the vehicle speed is estimated as shown in Equation (4).

$$u_n(t+\Delta t) = \frac{-c_1 + c_3 u_f + \tilde{s}_n(t+\Delta t) - \sqrt{[c_1 - c_3 u_f - \tilde{s}_n(t+\Delta t)]^2 - 4c_3[\tilde{s}_n(t+\Delta t)u_f - c_1 u_f - c_2]}}{2c_3}$$

(4)

where $\tilde{s}_n(t)$ is the predicted vehicle spacing at time *t* considering that vehicle *n* continues at its current speed where $\tilde{s}_n(t+\Delta t) = s_n(t) + [u_{n-1}(t) - u_n(t)]\Delta t + 0.5a_{n-1}(t)\Delta t^2$ where $a_n(t)$ is the acceleration of vehicle *n* at time *t*.

Collision Avoidance Modeling

In the case that the following vehicle is traveling at a higher speed than the lead vehicle (non-steady state conditions) the vehicle spacing should be sufficient to allow the following vehicle (vehicle *n*) to avoid a collision with the lead vehicle (vehicle $n-1$) if it were to decelerate at a feasible deceleration level. This deceleration level is assumed to be equal to $\mu f_b \eta_b g$, where μ is the coefficient of roadway friction, f_b is the driver brake pedal input [0,1], η_b is the brake efficiency [0,1], and g is the gravitational acceleration (9.8067 m/s^2). The resulting minimum vehicle spacing and the vehicle speed can be computed using Equations (5) and (6).

$$\tilde{s}_n(t+\Delta t) = \frac{1}{k_j} + \frac{u_n(t+\Delta t)^2 - u_{n-1}(t+\Delta t)^2}{25920\mu f_b \eta_b g} \quad (5)$$

$$u_n(t+\Delta t) = \sqrt{u_{n-1}(t+\Delta t)^2 + 25920\mu f_b \eta_b g\left(\tilde{s}_n(t+\Delta t) - \frac{1}{k_j}\right)} \quad (6)$$

Vehicle Acceleration Modeling (Vehicle Dynamics Model)

Vehicle acceleration can be modeled in two different ways: using a vehicle dynamics model or using a vehicle powertrain model. The vehicle dynamics approach approximates the vehicle for a point mass and ignores any gear-shifting effects on vehicle modeling. A vehicle powertrain approach requires more computations given that it models the vehicle gearbox. For simplicity the vehicle dynamics model is only considered.

Vehicle acceleration may be modeled considering the vehicle as a point mass and only considering the various forces acting on the vehicle. Vehicle dynamics models compute the maximum vehicle acceleration levels from the resultant forces acting on a vehicle (mainly vehicle tractive forces which is a function of the driver throttle input and resistance forces).

The vehicle tractive effort can be computed using Equation (7). Rakha and Lucic [34] introduced the β factor into Equation (7), in order to account for the gear shift impacts at low traveling speeds when trucks are accelerating. This factor is set to 1.0 for light duty vehicles [35]. The $f_p(t)$ factor models the driver throttle input level and ranges from 0.0 to 1.0. The

vehicle resistance force is calculated as the sum of the aerodynamic, rolling, and grade resistance forces acting on the vehicle [34, 36], as demonstrated in Equation (8).

$$F_n(t) = \min\left(3600 f_p(t) \beta \eta_d \frac{P_n}{u_n(t)}, m'_n g \mu\right) \quad (7)$$

$$R_n(t) = \frac{\rho}{25.92} C_d C_h A_f u_n(t)^2 + m_n g \frac{c_{r0}}{1000}\left(c_{r1} u_n(t) + c_{r2}\right) + m_n g G(t) \quad (8)$$

where $F_n(t)$ is vehicle tractive forces at time t (N); $f_p(t)$ is the driver throttle input at time t [0,1] (unitless); β is the gear reduction factor (unitless); η_d is the driveline efficiency (unitless); P is the vehicle power (kW); m'_n is the mass of vehicle n on its tractive axle (kg); g is the gravitational acceleration (9.8067 m/s^2); μ is the coefficient of road adhesion or the coefficient of friction (unitless); $R_n(t)$ is vehicle resistance force at time t (N); ρ is the air density at sea level and a temperature of 15°C (1.2256 kg/m^3); C_d is the vehicle drag coefficient (unitless), typically 0.30; C_h is the altitude correction factor (unitless) which is computed as C_h=1-0.085H where H is the altitude (km); A_f is the vehicle frontal area (m^2); c_{r0} is the rolling resistance constant (unitless); c_{r1} is the rolling resistance constant (h/km); c_{r2} is the rolling resistance constant (unitless); m_n is the total vehicle mass (kg); and $G(t)$ is the roadway grade at instant t (unitless). The rolling resistance parameters vary as a function of the road surface type, condition, and vehicle tires [36]. Generally, radial tires provide a resistance that is 25 percent less than that for bias ply tires. Typical values of vehicle frontal areas for different vehicle types and typical drag coefficients are provided in the literature [36]. Similarly typical values for the coefficient of roadway adhesion and the rolling resistance coefficients are provided in the literature [34, 36].

The vehicle acceleration is calculated as a ratio of the difference between the tractive and resistance forces divided by the vehicle mass (i.e., a=(F-R)/m). The vehicle speed ($u_n(t+\Delta t)$) and position ($x_n(t+\Delta t)$) at t+Δt is then computed using a first-order Euler approximation, as demonstrated in Equation (9) and (10).

$$u_n(t+\Delta t) = u_n(t) + 3.6 \frac{F_n(t) - R_n(t)}{m} \Delta t \quad (9)$$

$$x_n(t+\Delta t) = x_n(t) + u_n(t) \Delta t \quad (10)$$

Proposed Algorithm

The proposed algorithm is illustrated in Figure 2. The model starts with driver input of a target speed, a speed range, and car-following spacing threshold. Typically, the target speed is based on the roadway speed limit. The speed range is set to the maximum and minimum speed the driver is willing to accept. Finally, the car-following spacing threshold is based on driver or passengers' comfort.

Alternatively, the system can locate the vehicle on a high-resolution digital map to identify the desired speed based on the roadway speed limit. Using the road's topographic information, the system estimates the optimal speed profile that minimizes the vehicle fuel consumption within the target speed range. The optimal control estimates the throttle position and brake level that generates the desired speed profile while maintaining a safe following headway and spacing between the subject vehicle and a vehicle ahead of it. The model

utilizes the vehicle powertrain model that was described earlier to compute the feasible gear and speed range for use in the optimization algorithm.

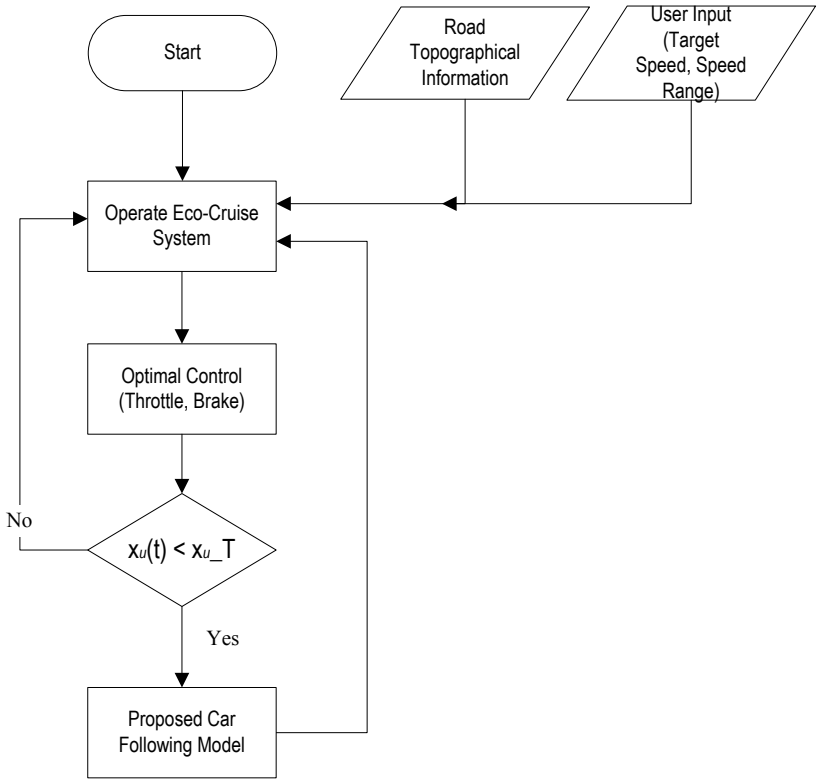

FIGURE 2 Proposed Eco-Drive Algorithm Logic.

The proposed logic can be summarized as follows:

1. If the spacing between the subject and lead vehicle is greater than the car-following threshold ($x_{u\_}T$), proceed to step 3. Otherwise, proceed to step 2.
2. Estimate the maximum vehicle acceleration at instant t based on the steady-state car-following model and collision avoidance constraints. Considering the Van Aerde functional form, the first step entails computing the maximum speed ($\hat{u}_n(t+\Delta t)$) at $t+\Delta t$ using equation (11). The maximum acceleration ($\hat{a}_n(t)$) is then computed using equation (12), and the maximum speed ($u_n(x_t + d_s)$) at the end of the first stage (position x_t+d_s) can then be computed using the equation (13). Proceed to step 4.

$$\hat{u}_n(t+\Delta t) = \min\left(\begin{array}{c} \dfrac{-c_1 + c_3 u_f + \tilde{s}_n(t) - \sqrt{[c_1 - c_3 u_f - \tilde{s}_n(t)]^2 - 4c_3[\tilde{s}_n(t)u_f - c_1 u_f - c_2]}}{2c_3} \\ \sqrt{u_{n-1}(t+\Delta t)^2 + 25920\mu f_b \eta_b g\left(s_n(t) - \dfrac{1}{k_j}\right)} \end{array}\right) \quad (11)$$

$$\hat{a}_n(t) = \frac{\hat{u}_n(t+\Delta t) - u_n(t)}{\Delta t} \quad (12)$$

$$u_n(x_t + d_s) = \sqrt{u_n(x_t)^2 + 2\hat{a}_n(t)d_s} \quad (13)$$

3. Using the DP algorithm described earlier, the optimal vehicle speed trajectory over the look-ahead distance (d_o) is estimated considering a spatial discretization of d_s (stage length). The maximum car-following speed constraint that was computed in step 2 is considered in identifying the search space of stage 1.
4. Move the vehicle and then go back to step 1 at the conclusion of time step Δt. Otherwise, end the simulation at $t=T$.

Simulation results

This section describes the simulation results of the proposed eco-drive system. The computer simulation software, MATLAB, was utilized to develop and evaluate the performance of the proposed system. Key input variables for the proposed system include the car-following spacing threshold; the car-following model parameters such as the free-flow speed, jam density, speed-at-capacity, and capacity parameters; vehicle data including powertrain-related data and fuel economy data; roadway topography data; real-time location data; and lead vehicle location data (or spacing data). In the simulated eco-driving system, the subject vehicle is alternatively operated in either the predictive eco-cruise control mode or the car-following mode. The default operational model of the system is the ECC system. However, the vehicle is operated in the car-following mode if the spacing between the subject and lead vehicle was within the car-following threshold. The following sections describe the various sensitivity tests performed to study the impact of the proposed eco-drive system.

Different Car-Following Thresholds

ECC systems optimize vehicle speed to minimize fuel consumption and GHG emissions. However, the typical ECC system assumes that the ECC vehicle does not interact with other vehicles, requiring drivers to operate ECC vehicles with caution to avoid collisions. The proposed ECC system integrates a car-following logic that includes a collision avoidance algorithm to improve safety while at the same time minimizing the vehicle fuel consumption level.

This section describes the impacts of using different car-following thresholds and parameters on the proposed system performance. The proposed system operates either in the ECC or car-following mode. The research investigates three car-following thresholds: 100 m, 50 m, and 30 m.

Figure 3 illustrates the speed profile of a lead vehicle and altitude data along the study section. The research used a 22-km section of I-81in southwestern Virginia, between mileposts 132 (Roanoke, Virginia) and 118 (Christiansburg, Virginia), which ranges from an elevation of 350 to 629 m above mean sea level. The maximum grade along the study section is 4 percent, and the maximum downhill grade is -5 percent, with an average grade of 0.6 percent.

The speed data were collected from the lead vehicle, a 2007 Chevy Malibu, using an OBD II data logger that also collected GPS signals. The drivers were instructed to maintain the target speed of 104 km/h (65 mi/h) without using cruise control. However, the figure shows that manual driving causes significant speed variations [37].

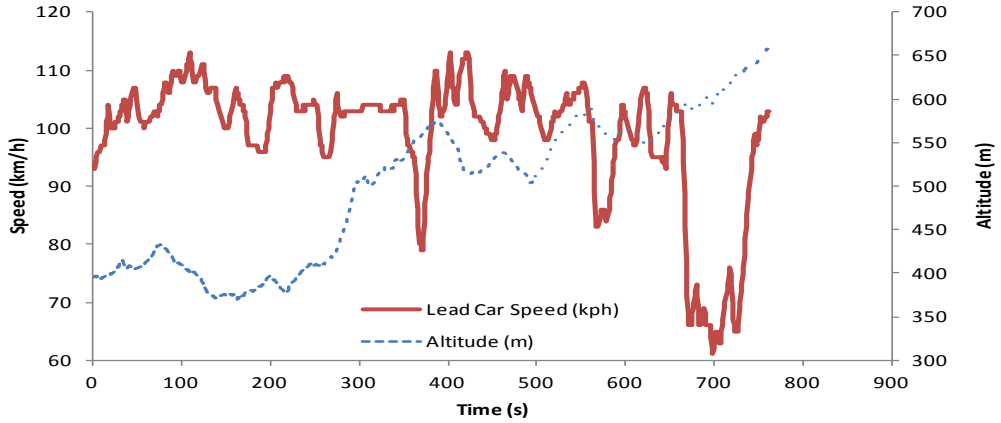

(a) Lead vehicle speed profile of Chevy Malibu

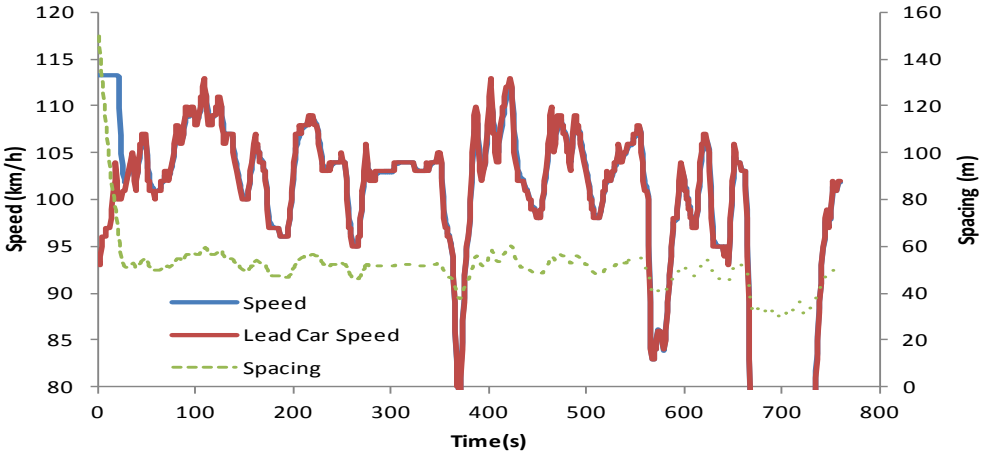

(b) Car-following-only speed & spacing profiles

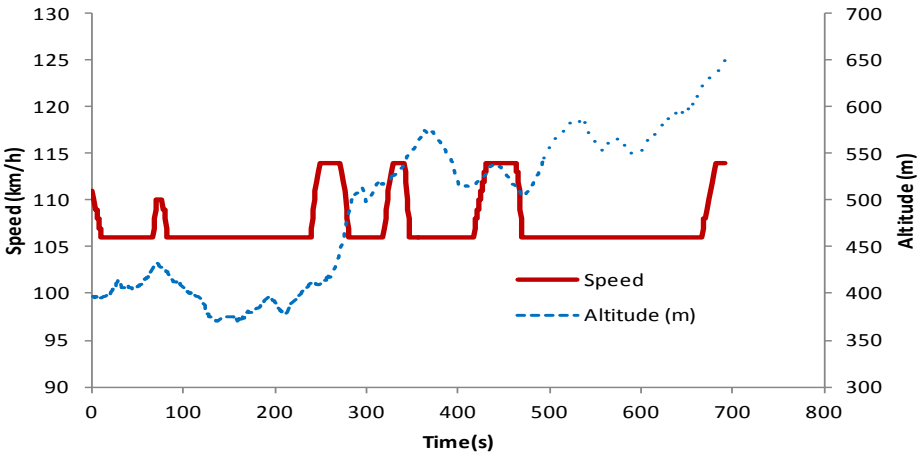

(c) Eco-cruise control only operation

FIGURE 3 Car-following and ECC operations, Toyota Camry.

Figure 3 also demonstrates the proposed car-following operation on the study section of I-81. The test vehicle was a 2011 Toyota Camry, which has a 2.4-L engine and 8.93 and 13.2 kilometer per liter (21 and 31 mpg) for city and highway fuel economy, respectively. As illustrated in the figure, the test vehicle followed the lead vehicle almost exactly, with an average vehicle spacing of 50 m. When the lead vehicle slowed, the proposed car-following algorithm reduced the spacing. The test vehicle generated a fuel economy of 5.7 Km/L (13.5 mpg) on the study section, which is significantly lower than the posted fuel economy data due to the multiple major upgrade segments of the I-81 study section.

A vehicle trip was simulated with the predictive ECC system at a target speed of 104 km/h (65 mi/h). For the predictive system, the vehicle was allowed to vary its speed by ± 8 km/h (± 5 mi/h) from the target speed. As shown in Figure 3, the predictive ECC system varied the vehicle speed using the topographical information. The results clearly illustrate that the test vehicle was controlled to maintain the lowest speed within the speed window on the uphill sections when the predictive control system was engaged. Furthermore, the speed was highest on the downhill sections because the predictive system attempted to maximize the use of gravitational energy. The test vehicle generated a fuel economy of 10.5 Km/L (24.6 mpg) on the study section, which is significantly greater than in the car-following-only mode of operation. Specifically, the ECC operation increased the fuel economy of the test vehicle, a 2011 Toyota Camry, by up to 82 percent compared to the car-following-only mode of operation.

The two control strategies represent the two extreme conditions. The first is a full car-following model with no ECC control while the second strategy represents an ECC system with no interaction with the surrounding traffic. Consequently, the next step entails considering a combination of car-following and ECC operational modes.

Figure 4 illustrates the simulated speed profiles for different car-following thresholds considering a 2011 Toyota Camry vehicle. As shown, the car-following threshold setting significantly affects the vehicle speed profiles. For the 100-m car-following threshold, the test vehicle is mostly engaged in the car-following mode (98.7 percent of the trip) and the speed profile is almost identical to that of the lead vehicle. During the trip, the test vehicle consumed 3.7 L of fuel, with a fuel economy of 5.7 Km/L (13.5 mpg) over the trip. The figure also illustrates the speed profile of the 50-m car-following threshold simulation run. The vehicle speed profile is notably different from that of the 100-m car-following threshold. When the test vehicle adopts the 50-m car-following threshold, the speed profile of the test vehicle differs from that of the lead vehicle but finds an optimal speed profile. The simulation results demonstrate that the test vehicle operates in the ECC mode for 85 percent of the trip and engages in the car-following mode of operation for only 15 percent of the trip. Also, when using the 50-m car-following threshold, the test vehicle improves its fuel economy to 6.8 Km/L (16.0 mpg), which is an 18 percent improvement over the car-following-only mode and the 100-m car-following threshold system operation. The figure also illustrates the speed profile of the 30-m car-following threshold. The simulation results show that the test vehicle undergoes two significant speed reductions at times 75 s and 485 s. These were caused by the spacing between the lead and subject vehicle falling below the collision avoidance distance. For the 30-m car-following threshold case, the test vehicle utilizes the ECC mode for most of the trip (97 percent) and improves its fuel economy to 8.7 Km/L (20.5 mpg).

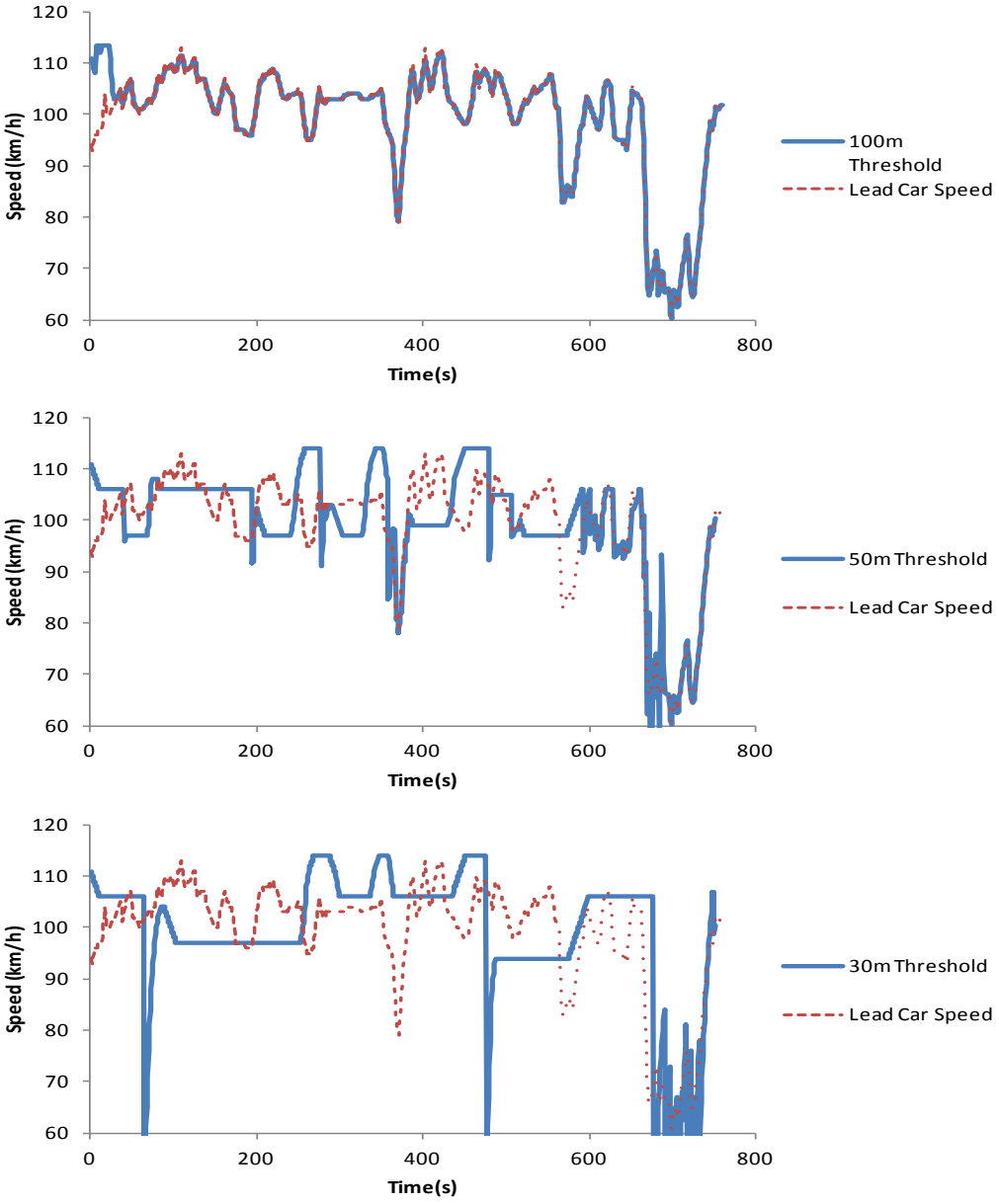

FIGURE 4 Various car-following thresholds, Toyota Camry.

Table 1 summarizes the simulation results of two other vehicles, a 2008 Chevy Tahoe and a 2008 Chevy Malibu Hybrid. The results demonstrate that ECC-only operation can significantly improve fuel efficiency compared to car-following mode of operation. Furthermore, as described earlier, the test vehicles attained the best fuel economy while interacting with the lead vehicles on the test road for the 30-m car-following threshold. Based on the simulation runs, the proposed system improves the fuel efficiency of the Toyota Camry, Chevy Tahoe, and Malibu Hybrid by up to 51, 21, and 31 percent, respectively. In conclusion, the results demonstrate that the proposed eco-drive system can significantly improve vehicle fuel economy on the tested roadway section.

TABLE 1 Summary of results of improved fuel efficiency

Method	Toyota Camry	Chevy Tahoe	Chevy Malibu Hybrid
Car-following only	5.7 Km/L	3.7 Km/L	6.8 Km/L
Eco-cruise only	10.4 Km/L (82%)	6.0 Km/L (60%)	10.7 Km/L (57%)
100-m Following Threshold	5.7 Km/L (-0.6%)	3.7 Km/L (-2%)	6.8 Km/L (-0.1%)
50-m Following Threshold	6.7 Km/L (18%)	4.0 Km/L (8%)	8.1 Km/L (19%)
30-m Following Threshold	8.6 Km/L (51%)	4.5 Km/L (21%)	8.9 Km/L (31%)

Figure 5 illustrates how different car-following threshold settings affect the spacing between the lead vehicle and the test vehicle. The shorter car-following threshold typically increases the inter-vehicle spacing while considerably improving fuel efficiency. The results demonstrate that when the Toyota Camry operates with the 30-m car-following threshold, the maximum spacing between the test vehicle and the lead vehicle increases to a maximum spacing of 450 m with an average spacing of 196 m for the entire trip. However, the 100-m and 50-m car-following thresholds reduce the average vehicle spacing for the Toyota Camry to 50 m and 78 m, respectively. The figure also illustrates the spacing profiles of the Chevy Tahoe. While the maximum and average spacing values of the Chevy Tahoe are smaller than those of the Toyota Camry, the results demonstrate that the maximum spacing value (230 m) for the 30-m car-following threshold is relatively higher than is typically found in normal highway driving conditions. Longer spacing between vehicles reduces the capacity of the road and also causes frequent lane changing and cut-in maneuvers.

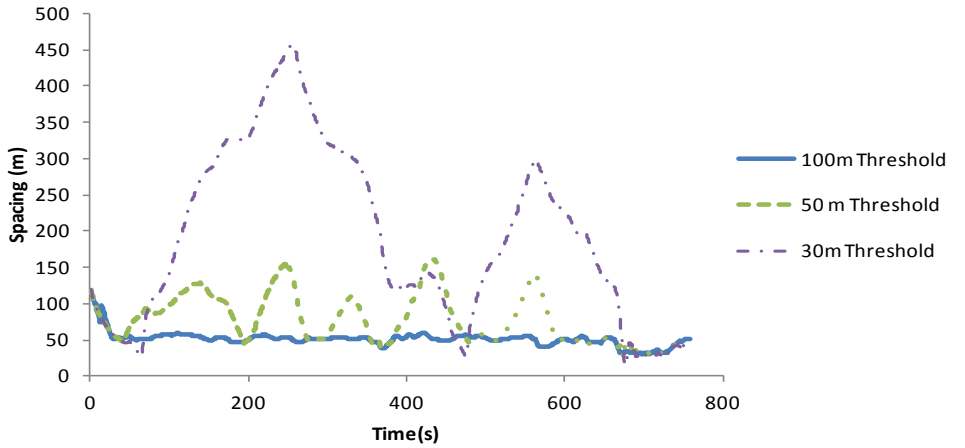

(a) Toyota Camry

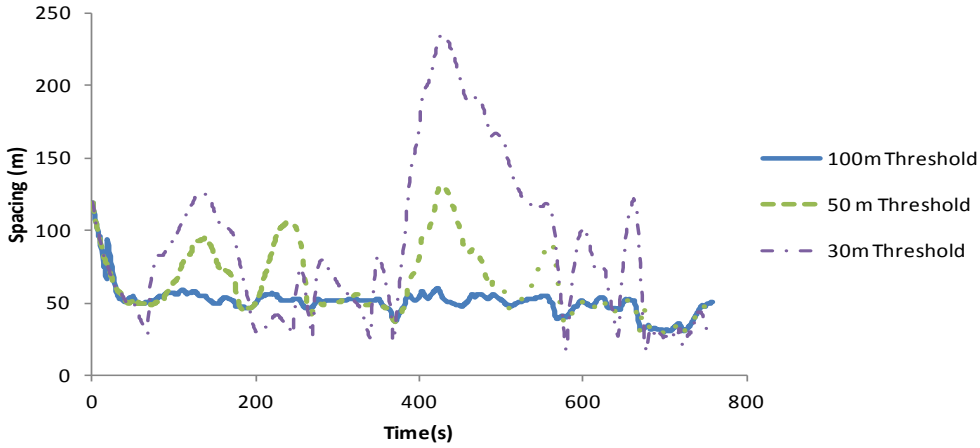

(b) Chevy Tahoe

FIGURE 5 Spacing of different car-following thresholds.

Dynamic Car-Following Thresholds

This section investigates a proposed dynamic car-following method to lessen the spacing between the lead and subject vehicles. The study proposed the dynamic threshold method which modifies the car-following threshold based on the vehicle spacing and the vehicle speed. First, the system compares the vehicle spacing and a pre-set maximum spacing limit (or 3 seconds headway based on the subject vehicle's speed). The 3 second headway was selected based on various sensitivity studies. If the spacing is greater than the 3 seconds headway, the system converts the ECC operational mode into the car-following mode in order to reduce the vehicle spacing. Otherwise, the vehicle is operated with ECC mode. Second, the system increases the car-following threshold based on the vehicle spacing. So as

spacing increases, the car-following threshold also increases. In particular, the dynamic car-following threshold is increased 20 percent when each time the vehicle spacing is greater than 3 seconds headway. Alternatively, if the spacing is reduced below the initial car-following threshold, the dynamic car-following threshold is set to the initial car-following threshold. Note that the performance of the dynamic car-following threshold method may be affected by the speed profiles of the leading vehicles and the roadway geometric condition. However, authors found that the proposed method performs well on various scenarios.

Figure 6 compares the speed profiles of the fixed 30-m car-following threshold and dynamic 30-m car-following threshold with a maximum spacing of 3 seconds headway. Thus, if the vehicle spacing is greater than 3 seconds headway, the ECC operational mode is converted into the car-following mode in order to reduce the vehicle spacing. The test vehicle using the dynamic method generally follows the lead vehicle without experiencing sudden speed drops observed in the fixed car-following model approach. Table 2 demonstrates the simulation results of using the dynamic car-following threshold. The results show that the dynamic car-following threshold method significantly reduces the average vehicle spacing without notably reducing the vehicle fuel economy. Specifically, the average vehicle spacing is reduced from 78 m to 52 m for the 50-m initial car-following threshold and from 196 m to 47 m with the 30-m initial car-following threshold. The results show that the dynamic car-following method slightly reduces fuel economy for 30-m car-following case. In particular, the dynamic car-following threshold mode of operation decreases the vehicle fuel economy to 7.2 Km/L (16.9 mpg) from 8.6 Km/L (20.5 mpg) for 30-m car-following threshold. In the case of the 50-m car-following threshold, the fuel economy was improved to 7.2 Km/L (16.9 mpg) from 6.7 Km/L (16 mpg).

TABLE 2 Fuel economy, average and maximum spacing of dynamic car-following method

Method	Fixed Car- Following Threshold	Dynamic Car-Following
Car-Following only	5.7 km/L	NA
100 m Following Threshold	5.7 km/L (50 m, 60 m)	NA
50 m Following Threshold	6.7 km/L (78 m, 161 m)	7.2 km/L (52 m, 135 m)
30 m Following Threshold	8.6 km/L (196 m, 457 m)	7.2 km/L (47 m, 135 m)

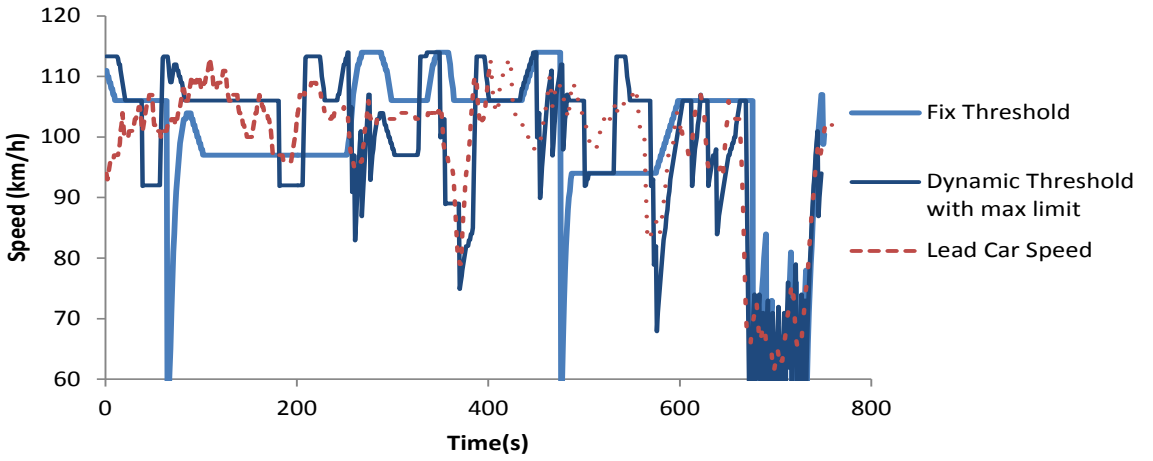

(a) Speed Profiles

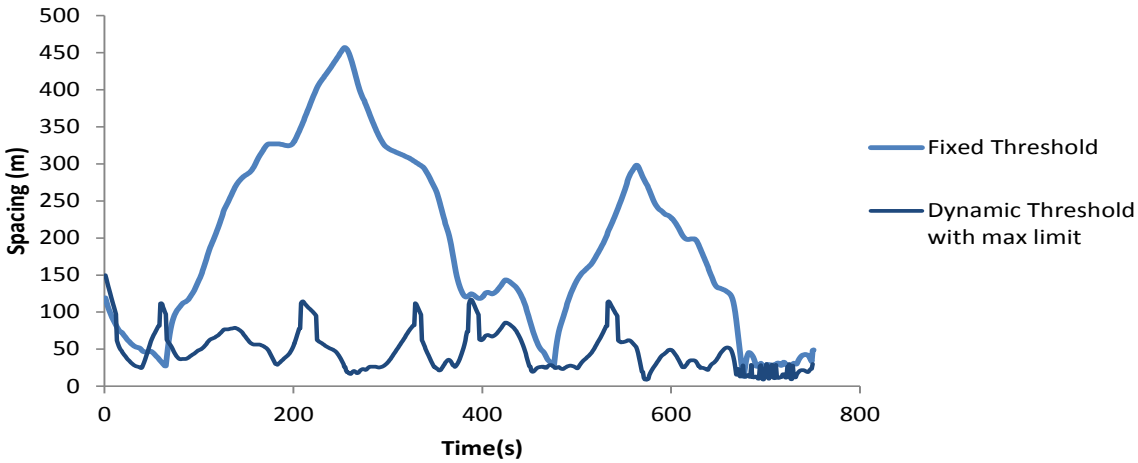

(b) Spacing

FIGURE 6 Dynamic car-following threshold results.

Impact of Maximum Throttle Level on System Performance

Because power levels significantly affect fuel consumption rates, reducing the maximum throttle level can dramatically improve the overall fuel efficiency of the proposed system. This study investigated the impact of constraining the maximum throttle level to 60 and 40 percent to quantify the fuel saving benefits compared to a 100 percent maximum throttle level (Table 3).

TABLE 3 Summary of results for different throttle levels, Toyota Camry.

Method	*100% Throttle*	*60% Throttle*	*40% Throttle*
Car-following only	5.7 km/L	6.7 km/L (16%)	8.5 km/L (49%)
Eco-cruise only	10.4 km/L (82%)	NA	NA
100-m following threshold	5.7 km/L (-0.6%)	6.7 km/L (16%)	8.5 km/L (49%)
50-m following threshold	6.7 km/L (18%)	7.8 km/L (38%)	8.5 km/L (50%)
30-m following threshold	8.6 km/L (51%)	8.8 km/L (55%)	8.8 km/L (53%)

The simulation used the 2011 Toyota Camry as the test vehicle. The results show that even if the test vehicle utilizes the car-following-only mode on the I-81 study section, it can improve its fuel economy by 16 percent and 49 percent at 60 percent and 40 percent throttle levels, respectively. Using a 40 percent throttle level, the fuel economy of the test vehicle improves from 6.7 Km/L (16 mpg) to 8.5 Km/L (20.3 mpg) for the 50-m car-following threshold and from 8.6 Km/L (20.5 mpg) to 8.8 Km/L (20.8 mpg) for 30-m car-following threshold. Using a 40 percent throttle level improves the overall fuel efficiency, but it also produces longer vehicle spacings, as illustrated in Figure 7. When 40 percent throttle levels are employed in the proposed eco-drive system with a 50-m car-following threshold, the average spacing increases from 78 m to 99 m and the maximum spacing increases from 162 m to 277 m.

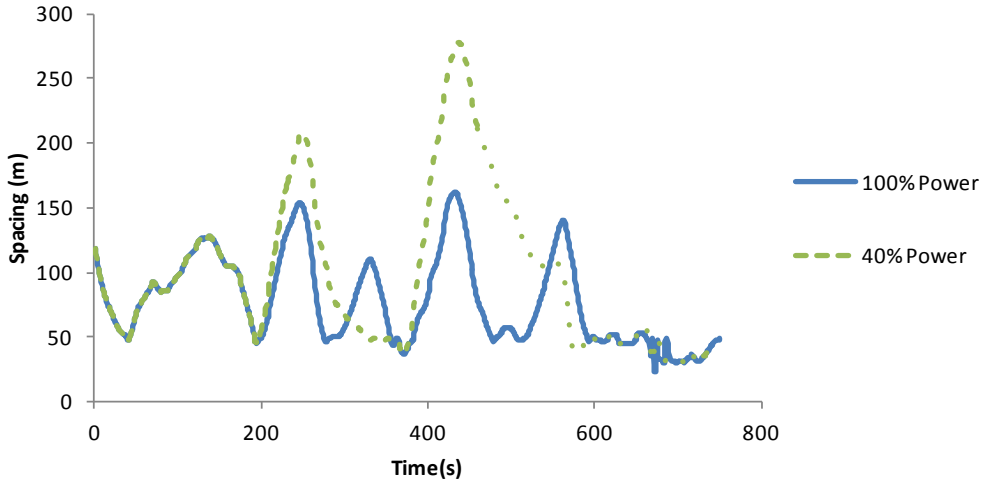

FIGURE 7 Spacing comparison of different power levels for Toyota Camry with 50-m threshold.

Benefits of Following an ECC-equipped Vehicle

This section investigates the benefits of following an ECC vehicle by putting the ECC vehicle in the lead position and a test vehicle in the following position using a car-following-only mode of operation.

Figure 8 illustrates the speed profiles of the lead ECC vehicle and the car-following vehicle, which utilizes the proposed car-following algorithm. The simulation results demonstrate that the test vehicle, a Toyota Camry, increases its fuel economy to 10.1 km/L (23.7 mpg) just by following the lead ECC vehicle without using any optimum controls. Note when the test vehicle is operated with the ECC-only mode, the test vehicle achieves a fuel economy of 10.5 Km/L (24.6 mpg). The study demonstrated that non-ECC-equipped vehicles can significantly reduce their own fuel consumption just by following a lead ECC-equipped vehicle. The result explains that the optimum operation of vehicle is a key factor of vehicle fuel saving.

The simulation studies of the Chevy Tahoe and Malibu Hybrid reveal similar results. The Chevy Tahoe and Malibu Hybrid achieve fuel efficiencies of 6.1 Km/L (14.3 mpg) and 10.3 Km/L (24.3 mpg), respectively, just by following a lead ECC vehicle on the study road section. The fuel efficiencies of the Chevy Tahoe and Malibu Hybrid under ECC operation are 6.1 Km/L (14.3 mpg) and 10.8 Km/L (25.4 mpg). The results confirm that the fuel-saving benefit of following an ECC vehicle is as great as using the ECC system.

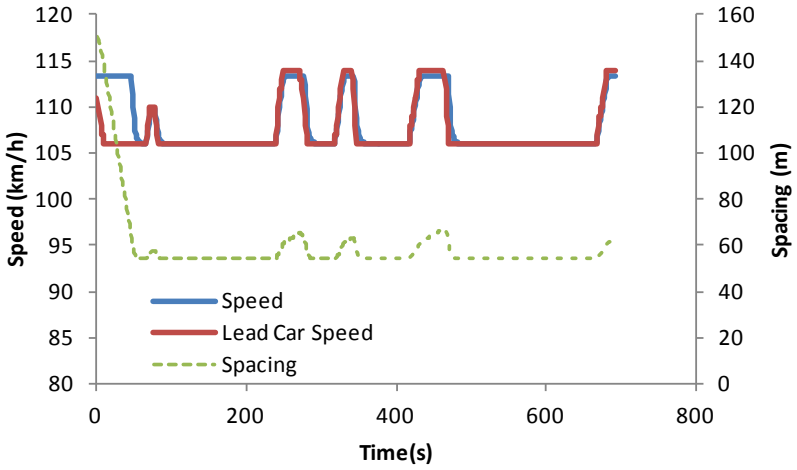

FIGURE 8 Following an ECC-equipped vehicle results.

ECO-LANES APPLICATIONS

This study utilizes the INTEGRATION microscopic traffic simulation software in order to evaluate Eco-Lanes applications. The following sections describe the fuel consumption and emission models that are implemented in the INTEGRATION software and the calibration efforts for the Eco-Lanes simulation model.

Model Calibration

This section describes the calibration efforts of the INTEGRATION simulation model. Figure 9 illustrates the study site. This heavily congested 24 km (or 15 mi) study section extends from Exit 47 (Manassas, Virginia, or A in Figure 1) to Exit 62 (Fairfax, Virginia, or B in Figure 1) of I-66 eastbound.

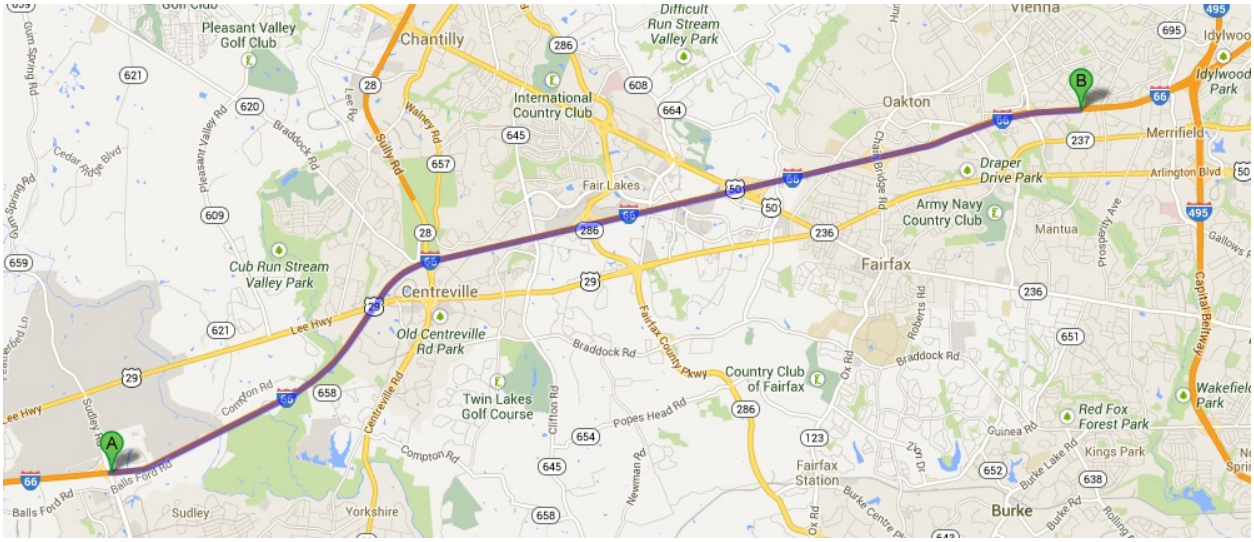

FIGURE 9 Study site (SOURCE: Google map).

A simulation model was constructed using traffic count and speed data that were collected during the a.m. peak hours (6:00 a.m. – 9:00 a.m.) from May 1 to May 3, 2012. These a.m. peak weekday (Tuesday, Wednesday, and Thursday) data represent congested roadway conditions on I-66 eastbound. Using the traffic count data, Origin-Destination (O-D) demand data were constructed using the QueensOD software (*24*). QueensOD was utilized to estimate the O-D tables using a maximum likelihood approach. QueensOD estimates O-D traffic demands using observed link traffic flows, observed link turning movement counts, and link travel times as input. A total of 36 O-D tables were generated in order to represent an O-D demand for every 5 minutes.

Figure 10 illustrates the speed-flow relationships at major locations on the study site. The four calibration sites (mileposts 51, 56, 59, and 62) were selected because these locations are frequently affected by severe congestion. Microscopic simulation software requires adjusting the model input parameters to obtain a realistic match between the field data and the model output. The macroscopic flow characteristics are typically associated with the

steady-state conditions. Thus, microscopic simulation software requires calibrating the parameters of the steady-state relationships (*25*). Traffic stream models relate three traffic stream measures: space-mean-speed (u), flow rate (q), and density (k). The models express the motion of a traffic stream by approximating the flow of a continuous compressible fluid. Various graphs showing each pair of space-mean-speed (u), flow rate (q), and density (k) are typically used to represent the steady-state properties of the traffic condition. Figure 10, which includes the speed-flow (u-q) relationships, demonstrates the steady-state properties of four different locations on I-66. The INTEGRATION model requires the calibration of various parameters, including the facility free-flow speed (km/h), roadway jam density (veh/km/lane), mean saturation flow rate (veh/h/lane), and speed-at-capacity (km/h). These parameters were estimated using the collected field data. Figure 10(d) illustrates that the traffic stream speed remains almost constant regardless of the flow rate because it is located in the uncongested regime.

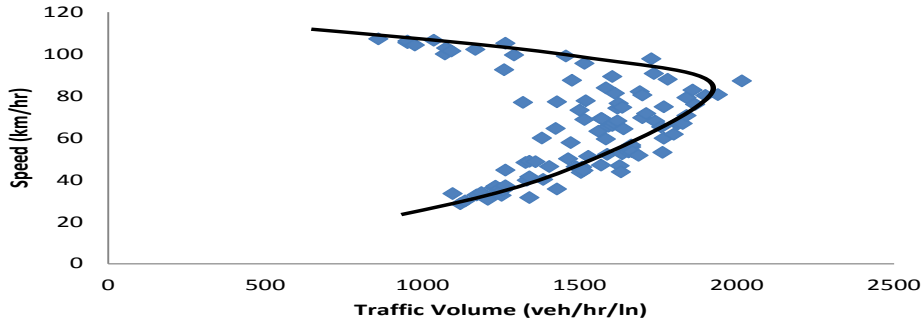

(a) Speed-flow (u-q) relationship at I-66 mile post 51

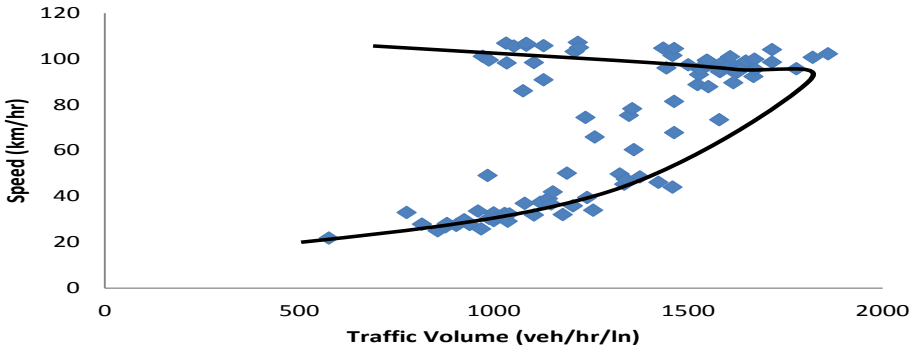

(b) Speed-flow (u-q) relationship at I-66 mile post 56

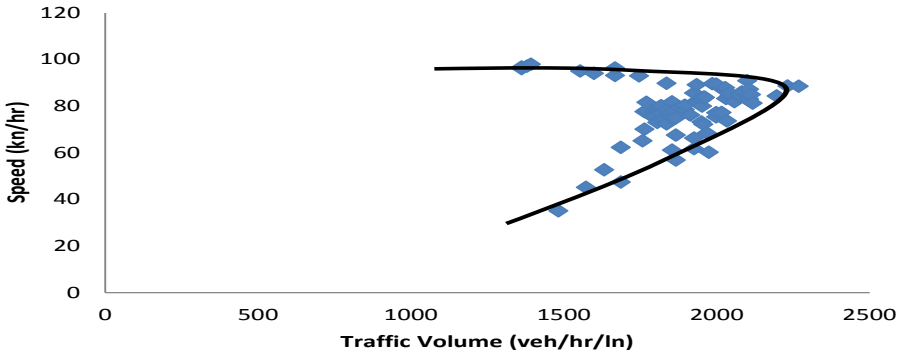

(c) Speed-flow (u-q) relationship at I-66 mile post 59

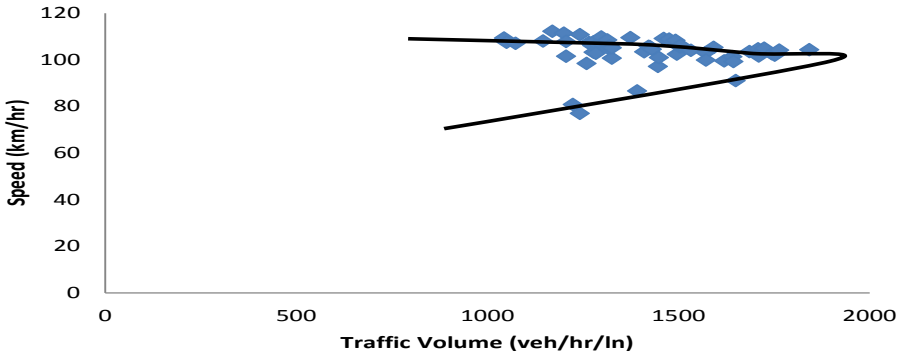

(d) Speed-flow (u-q) relationship at I-66 mile post 62

FIGURE 10 Speed-flow (u-q) relationship of field data.

Figure 11 illustrates the calibration results of the four sites. The figure shows the mean speeds obtained from the simulation model's output and the maximum and minimum speeds of the observed field data. Since this study utilized field data that were collected on three weekdays, the mean values of field data were generally located between the maximum and minimum speeds of the measured field data. This study utilized maximum and minimum speed values since only three days of data were available. The figure demonstrates that the speed values of the calibrated model generally follow the pattern of measured speed data. Also, the speed values of the simulation are mostly located within the maximum and minimum values of the field data except for a few cases. In particular, Figure 11(b) illustrates that the simulation reasonably follows a significant speed drop observed from the field data. The relative average speed differences of the simulation and the field data were 7.5%, 0.4%, 3.3%, and 14.8% for mileposts 51, 56, 59, and 62, respectively.

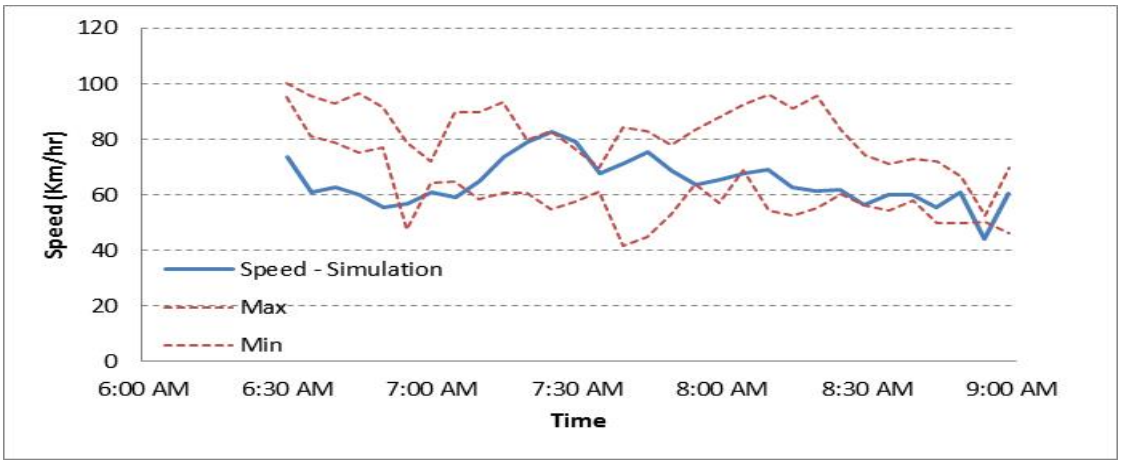

(a) Speed comparison at I-66 mile post 51

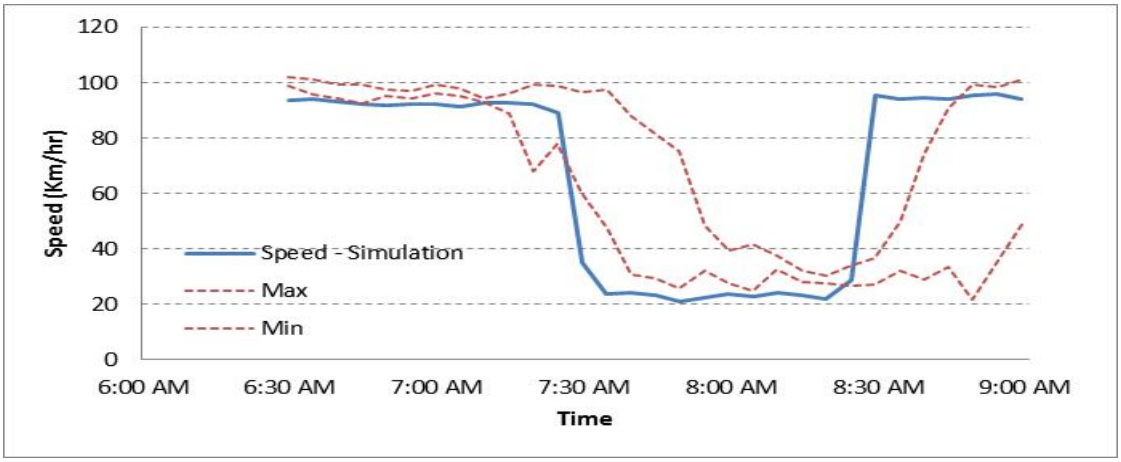

(b) Speed comparison at I-66 mile post 56

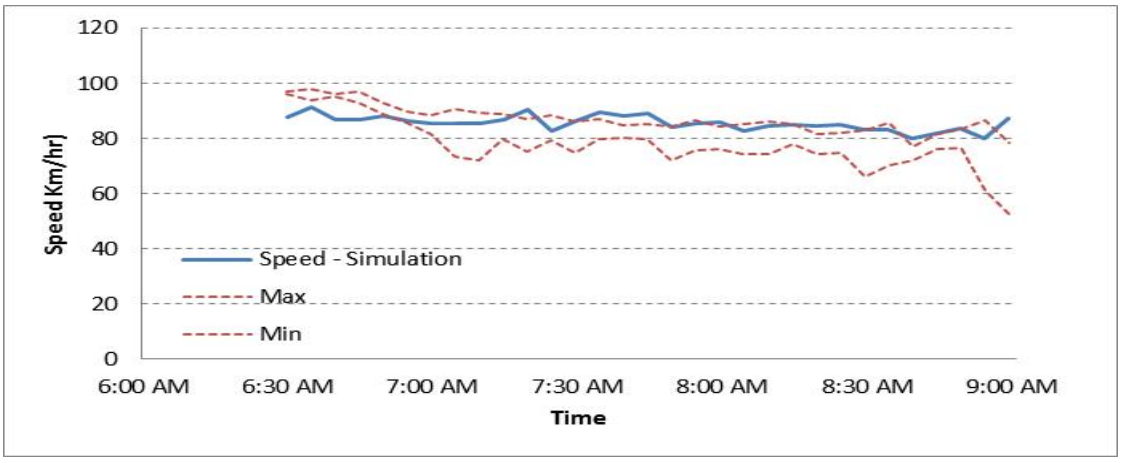

(c) Speed comparison at I-66 mile post 59

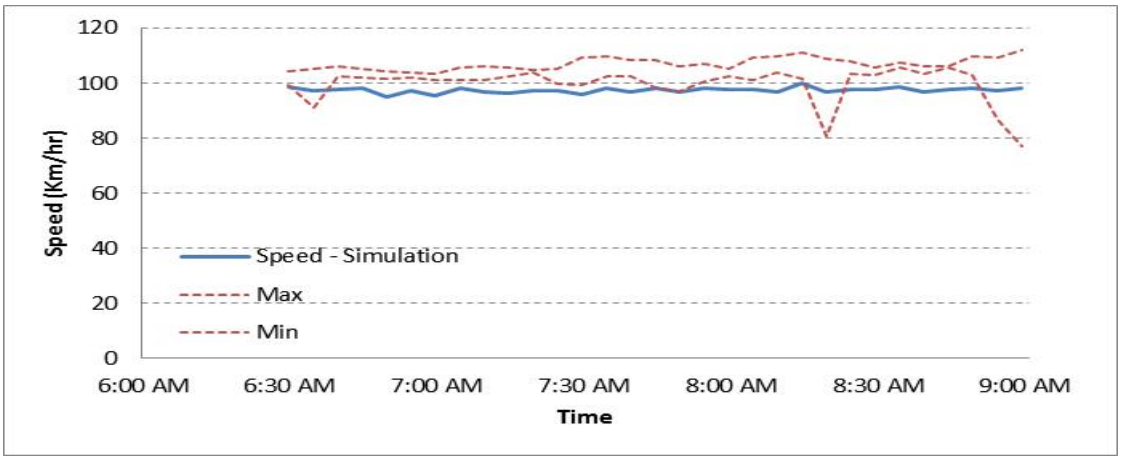

(d) Speed comparison at I-66 mile post 62

FIGURE 11 Calibration results.

ECO-LANES APPLICATIONS

This section investigates the feasibility of Eco-Lanes applications using the INTEGRATION microscopic simulation software. Typical eco-lanes on highways are utilized by transit, high occupancy, low emission, alternative fuel vehicles, or regular vehicles operated using eco-driving methods. The optimized eco-speed is estimated by traffic control centers based on the data collected from roadside equipment and connected vehicles.

The detailed information flow diagram for Eco-Lanes applications is illustrated in Figure 12. Real-time traffic information, air quality data, and weather data from roadside equipment are transmitted to a traffic management center (TMC). Vehicle operational and environmental data from connected vehicles are also broadcast using V2I communication and transmitted to the TMC. The vehicle operational data include vehicle type, vehicle specification, real-time speed and acceleration, vehicle position, vehicle routing information, and historical driving behavior. The TMC provides the collected roadway information data to the eco-driving processing center, which processes the collected data. The eco-driving processing center determines the specifications for eco-lanes, and evaluates the feasibility and the benefits of the implementation of a specific Eco-Lanes application. The eco-driving processing center determines the eco-lanes specification based on historical data, real-time data, and predicted future traffic state data. The specifications for eco-lanes include eco-lanes criteria, the spatial and temporal eco-lanes boundaries, vehicle types allowed in the eco-lanes, and optimum vehicle operational criteria in the eco-lanes.

Once the eco-driving processing center determines the benefits of operating eco-lanes, the TMC transmits the specifications to connected vehicles via roadside devices. The TMC continuously monitors the traffic flow and the environmental data of the Eco-Lanes applications and manages their control strategies.

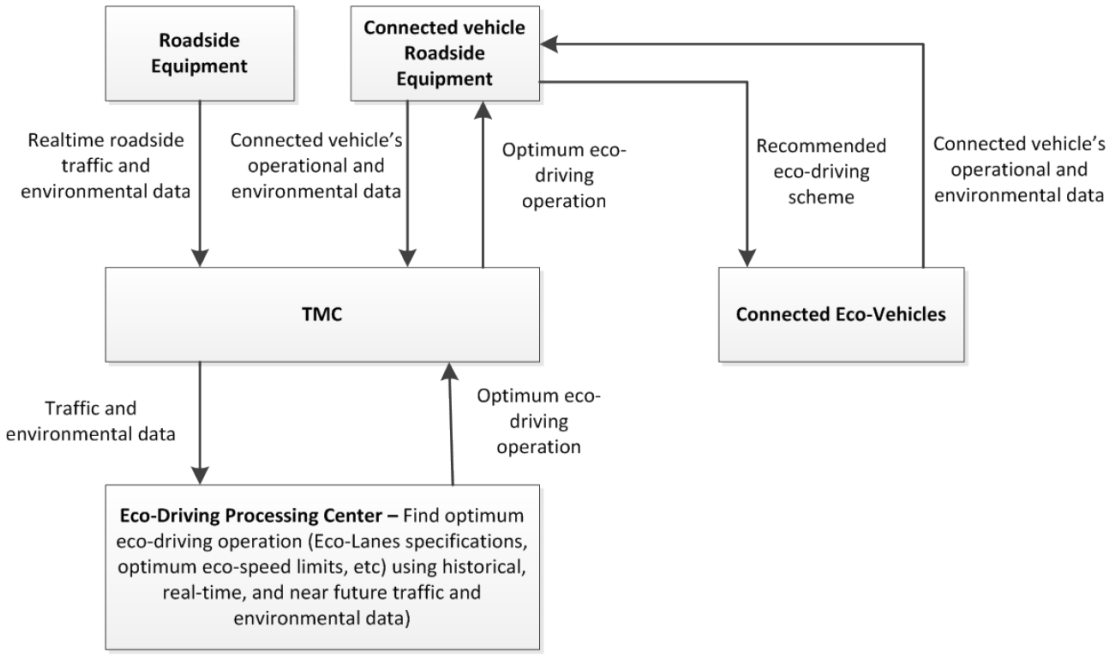

FIGURE 12 Information flow diagram of Eco-Lanes application.

Dynamic Eco-Lanes Operation

This scenario investigates the feasibility of dynamic Eco-Lanes application. In this scenario, drivers are required to operate the vehicle using mild acceleration levels to reduce transportation energy consumption and improve vehicle mobility. In particular, drivers can utilize up to 50% of maximum throttle level in the eco-lanes. A recent study found that high acceleration operations are responsible for a significant amount of total trip emissions and fuel consumption levels and that significant improvement in air quality and energy consumption are achievable by restricting vehicle high engine loads. In this scenario, eco-driving vehicles utilize one median lane as an eco-lane with a restricted acceleration capability.

This study only utilizes regular passenger cars (normal-emitting vehicles) in order to reduce the complexity of various vehicle compositions. Thus, low-emitting vehicles, high-emitting vehicles, and any alternative fuel vehicles are not considered in this scenario. In this scenario, in addition to eco-vehicles operating with restricted acceleration, non-eco-vehicles are able to use the eco-lanes without restricting their acceleration by using a car-following-only mode of operation. Recent research demonstrates that regular vehicles can benefit significantly by following a lead eco-drive vehicle. The study found that the fuel-saving benefits of following an eco-vehicle are as great as using the eco-driving system. In this scenario, the TMC detects major congestion at 6:30 a.m. and starts to operate eco-lanes at 6:30 a.m. Thus, no Eco-Lanes application is operated from 6:00 a.m. to 6:30 a.m., and the TMC sends a message to eco-vehicles to utilize the eco-lanes with 50% maximum throttle levels at 6:30 a.m.

Driver acceptance of the Eco-lanes system is an important measure in the operation of eco-lanes. While no study has been performed regarding eco-lanes, a recent study found that

the majority of participants agreed that a number of specific features of the connected vehicle technology would improve driving in the real world, and they would like to have connected vehicle features in their personal vehicles (*28*).

Figure 13 provides the results of a simulation of dynamic Eco-Lanes system. Approximately 31,400 vehicles were simulated on the I-66 study section for the 3-hour morning peak period (6:00 a.m. – 9:00 a.m.). Among the 31,400 vehicles, 1,744 vehicles (or 5.6%) were operated as eco-vehicles in the eco-lanes in this study. The simulation of the three-hour period was repeated 10 times with a different random seed in order to consider the stochastic properties of traffic. The total vehicle delay, travel time, fuel consumption, and emissions (HC, CO, NO_x, and CO_2) were extracted from output files and utilized as measures of effectiveness (MOEs).

Figure 13 illustrates that the Eco-Lanes system significantly improves the mobility, fuel efficiency, and air quality of the network except for NO_x emission. Typically, the highest levels of CO and HC are produced under fuel-rich conditions and the highest levels of NO_x are emitted under fuel-lean conditions. Fuel-rich operations typically occur under heavy engine loads, such as during rapid acceleration at high speeds and on steep upgrades.

Consequently, the Eco-Lanes system, which reduces high engine loads, may positively affect CO and HC but may increase NO_x. The simulation study also found that when the Eco-Lanes system is operated, the average vehicle (both eco-vehicles and non-eco-vehicles) can save 61 s (8.5%) in travel time against the base case scenario. In particular, the average travel time for the Eco-Lanes system was 10.95 min, while the average travel time of the base case was 11.96 min. Furthermore, the average delay per vehicle was reduced from 270 s to 208 s when the Eco-Lanes system was utilized. In the case of fuel consumption and emissions, the Eco-Lanes system reduced fuel consumption, HC, CO, and CO_2 emissions by 4.5%, 3.1%, 3.4%, and 4.6%, respectively, compared to the base case scenario. The study also found that the Eco-Lanes system increased NO_x emissions by 8%. In order to confirm the results, t-tests were performed at a 5% significance level assuming identical mean values for the results of the Eco-Lanes and base case. The t-test results (p-values of 0.001 and 0.001) indicate that the Eco-Lanes system does result in significant reductions in the network travel times and total delay. The t-tests for fuel consumption and emissions produced p-values of 0.000, 0.000, 0.000, 0.000, and 0.000 for fuel consumption, HC, CO, NO_x, and CO_2 emissions, respectively, which are statistically significant.

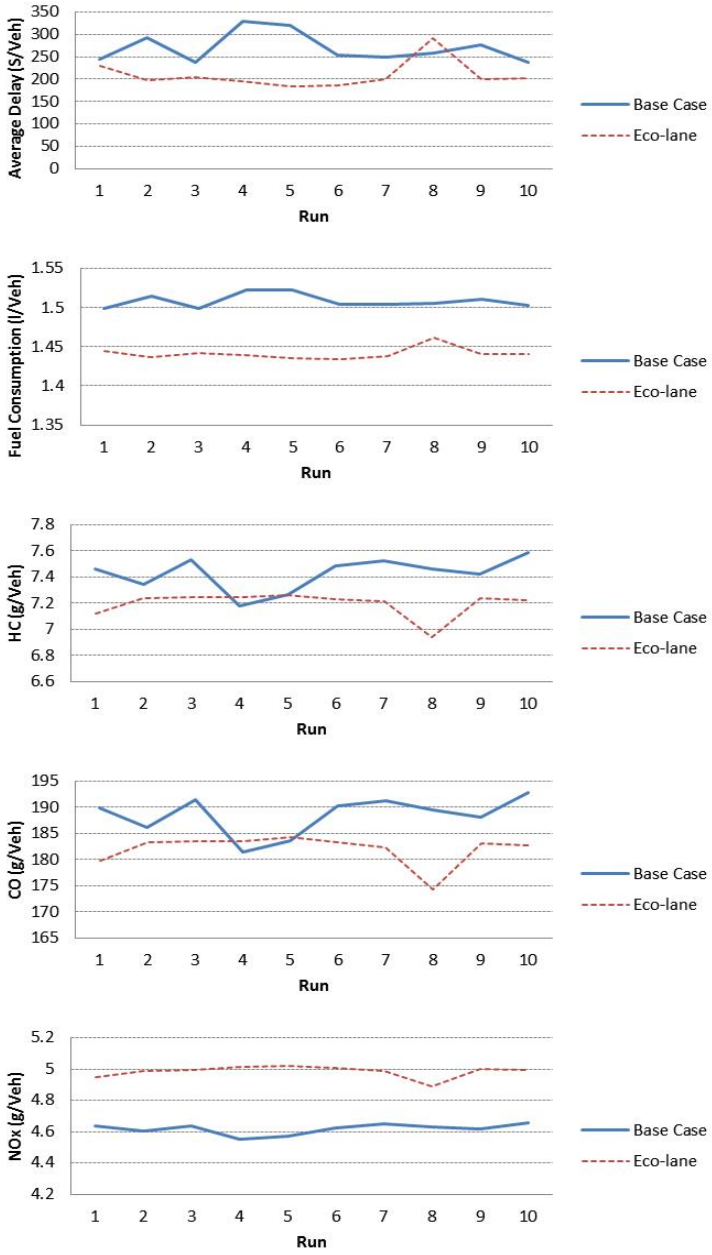

FIGURE 13 Eco-Lanes operation with 50% throttle levels.

Impact of Predictive Eco-Lanes Applications

Traffic state estimation and prediction are critical parts of traffic management and advanced traveler information systems. A key component of the predictive Eco-Lanes system entails predicting the onset of congestion before it occurs so that eco-lanes operation can be provided to approaching vehicles in order to reduce fuel consumption and congestion. In previous research, the research team developed a particle filter approach that can accurately predict freeway traffic conditions using measured traffic speed data.

In this scenario, the TMC predicts severe congestion at 6:30 a.m. and starts to operate eco-lanes 15 minutes (6:15 a.m. to 9:00 a.m.) or 30 minutes (6:00 a.m. to 9:00 a.m.) earlier than the congestion is predicted to occur on the study corridor. Out of 31,400 vehicles in the simulation, 1,900 vehicles (or 6.1%) and 2,000 vehicles (or 6.5%) were operated as eco-vehicles for the 15-minute predictive Eco-Lanes system and the 30-minute predictive Eco-Lanes system, respectively. The 30-minute predictive Eco-Lanes system utilized more eco-vehicles since the system started the eco-lanes 15 minutes earlier. For both systems, the eco-vehicles utilized 50% of maximum throttle levels.

Figure 14 illustrates the simulation results for predictive Eco-Lanes applications. The figure shows the 95 percent confidence limits and mean values of the MOEs. The simulation for the three-hour period was repeated 10 times with a different random seed. The figure illustrates that both the 30-minute predictive Eco-Lanes system and the 15-minute predictive Eco-Lanes system significantly reduce total travel time, total delay, and fuel consumption, as well as HC, CO, and CO_2 emissions, but increase NO_x emissions. In particular, the 30-minute predictive Eco-Lanes system reduces travel time, delay, fuel consumption, HC, CO, and CO_2 emissions by 10.7%, 28.7%, 5.3%, 3.4%, 3.7%, and 5.4%, respectively, compared with the base case scenario. The 15-minute predictive Eco-Lanes application reduces travel time, delay, fuel consumption, HC, CO, and CO_2 emissions by 8.6%, 23.0%, 4.7%, 3.4%, 3.7%, and 4.8%, respectively, compared to the base case scenario. Table 4 compares any significant differences between Eco-Lanes applications using t-tests. The statistical analysis concluded that there is no significant difference between the 30-minute predictive Eco-Lanes system and the 15-minute predictive Eco-Lanes system. Both predictive Eco-Lanes systems significantly reduce fuel consumption and CO_2 emissions compared with the original Eco-Lanes application. The t-test results also show that the predictive Eco-Lanes systems did not result in statistically significant changes in travel time, total delay, HC, and CO emissions.

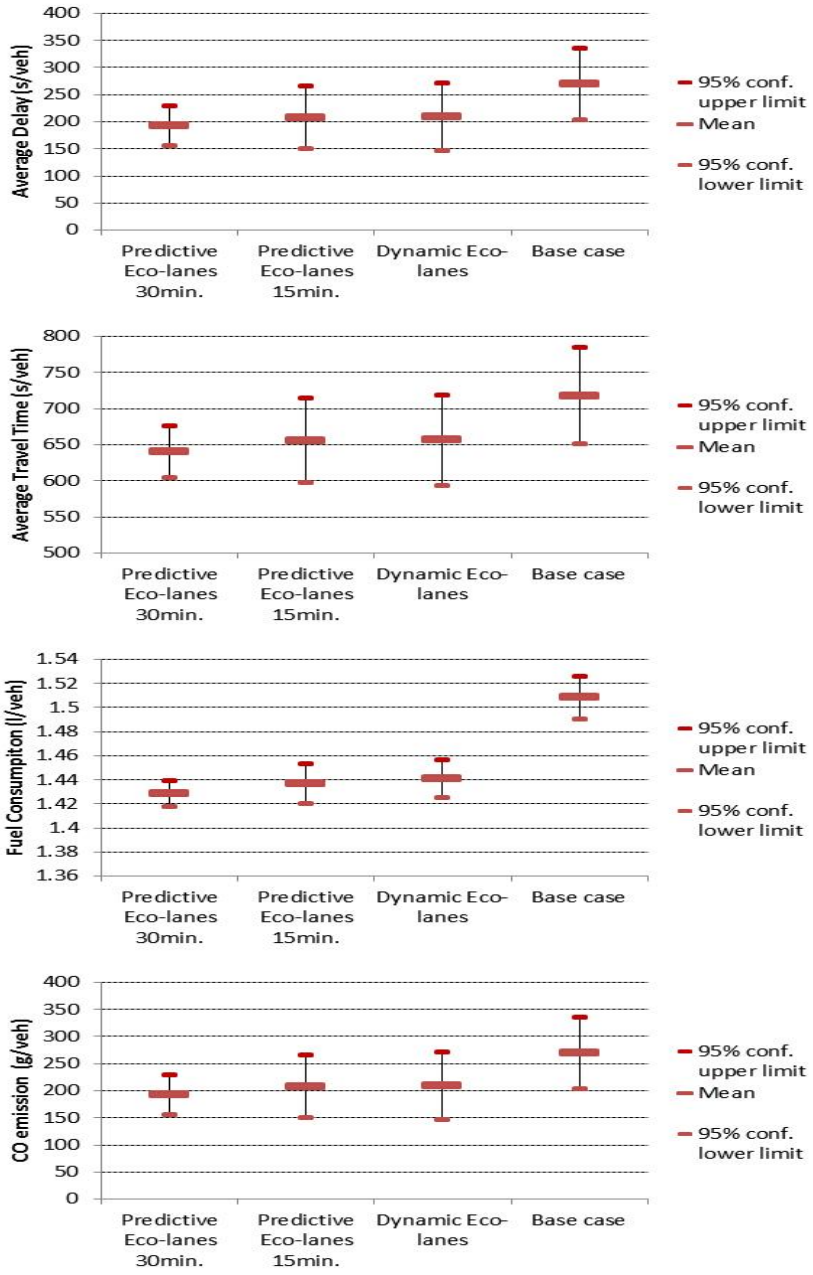

FIGURE 14 Predictive Eco-Lanes operation with 50% throttle levels.

TABLE 4 T-test Results (p-values) Comparing Eco-Lanes Systems

	Travel Time	Total Delay	Fuel	HC	CO	NO_x	CO_2
Eco-Lanes vs. Pred. Eco-Lanes 15 min.	0.180	0.179	0.016	0.906	0.923	0.016	0.029
Eco-Lanes vs. Pred. Eco-Lanes 30 min.	0.188	0.188	0.000	0.452	0.582	0.000	0.003
Pred. Eco-Lanes 15 min. vs. 30 min.	0.967	0.966	0.238	0.542	0.571	0.119	0.357

Impact of Maximum Throttle Levels on Eco-Lanes Applications

Because power levels significantly affect fuel consumption and emission rates, reducing the maximum throttle level can dramatically improve the overall fuel efficiency of the proposed system. This study investigated the impact of constraining the maximum throttle levels from 10% to 90%, as demonstrated in Table 5. Due to the stochastic nature of traffic, the simulations were repeated 10 times with different seeds to result in different model outcomes. The MOEs in the table are the mean values of 10 simulations. The 30-minute predictive Eco-Lanes system is utilized for all simulations. The simulation results demonstrate that for this specific network scenario, when eco-vehicles are operated at 50% maximum throttle level, the total network delay, travel time, fuel consumption, HC, CO, and CO_2 emissions are minimized on the study corridor.

TABLE 5 Impact of Different Maximum Throttle Levels on Eco-Lanes Operation

	Travel Time (s)	Total Delay (s)	Fuel (l/veh)	HC (g/veh)	CO (g/veh)	NO_x (g/veh)	CO_2 (g/veh)
Base Case (No Eco-Lanes)	717.86	270.14	1.51	7.43	188.47	4.62	3237.54
10% Throttle	727.55	279.22	1.46	7.48	188.76	4.84	3135.13
30% Throttle	646.54	198.41	1.43	7.18	181.50	5.07	3072.24
50% Throttle	640.75	192.68	1.43	7.17	181.43	5.05	3060.60
70% Throttle	661.24	213.18	1.43	7.12	180.05	5.00	3072.51
90% Throttle	665.64	217.59	1.43	7.11	179.72	4.99	3072.42

For this analysis, only one passenger vehicle type is utilized. However, various vehicle compositions may result in different optimum throttle levels. The table also shows that when the 10% throttle level is selected, the Eco-Lanes applications increases travel time and delay compared to the base case scenario.

Impact of Eco-speed Limits on Eco-Lanes Application

Speed reductions are commonly considered as an effective tool to reduce fuel consumption and emissions. In this scenario, TMC provides eco-speed limits that are optimized for mobility, fuel consumption, and emission levels. These eco-speed limits can be estimated based on historical, real-time, and near-future traffic and environmental data, including vehicle specification data.

This section investigates eco-speed limits for eco-vehicles in eco-lanes. The eco-speed limit is different from the target speed of SPD-HARM and VSL systems because eco-speed limits are only applied to eco-vehicles operating in eco-lanes. Thus, non-eco-vehicles are not affected by the eco-speed limit. However, in the case of SPD-HARM, all connected vehicles are recommended to use the optimum target speed in the predefined SPD-HARM sections. Also, the eco-speed limits are only applied in the eco-lanes, while the target speed of SPD-HARM is applied to all available lanes.

Table 6 demonstrates the impact of eco-speed limits on the Eco-Lanes system. The 30-minute predictive Eco-Lanes system was utilized and the eco-vehicles utilized 50% of the maximum throttle level with the eco-speed limits. The speed limit (or free-flow speed) was set to 104 km/h (65 mi/h) for all vehicles in the network. The simulation results show that the Eco-Lanes system has different optimum speed limits for different MOEs. Specifically,

travel time, total delay, fuel consumption, and CO_2 emission are minimized when a 104 km/h (65 mi/h) speed limit is applied to eco-vehicles. A 93.6 km/h (58.5 mi/h) speed limit (or 90% of the free-flow speed) reduces HC and CO emissions. The table shows that using low speed limits such as 62.4 km/h (39 mi/h) and 52 km/h (32.5 mi/h) (or 60% and 50% of free-flow speed) may increase travel time, delay, fuel consumption, and most emission levels, even when the Eco-Lanes system is operated.

TABLE 6 Impact of Different Maximum Vehicle Speeds for Eco-vehicles on Eco-Lanes Operation

	Travel Time (s)	Total Delay (s)	Fuel (l/veh)	HC (g/veh)	CO (g/veh)	NO_x (g/veh)	CO_2 (g/veh)
Base Case (No Eco-Lanes)	717.86	270.14	1.51	7.43	188.47	4.62	3237.54
Max. speed 104 km/h	640.75	192.68	1.43	7.17	181.43	5.05	3060.60
Max. speed 93.6 km/h	706.87	258.71	1.44	6.97	175.22	4.92	3100.48
Max. speed 83.2 km/h	700.15	251.87	1.44	7.12	179.55	4.83	3089.69
Max. speed 72.8 km/h	667.49	219.17	1.45	7.65	193.82	4.89	3088.00
Max. speed 62.4 km/h	735.85	287.47	1.49	8.06	202.29	4.93	3181.14
Max. speed 52 km/h	746.20	297.76	1.52	8.64	215.39	5.04	3228.48

NOTE: 1 mi/h = 1.6 km/h.

Eco-Lanes Operation with SPD-HARM

The objective of SPD-HARM is to dynamically adjust and coordinate maximum appropriate vehicle speeds in response to downstream congestion, incidents, and weather or road surface conditions in order to maximize traffic throughput and reduce vehicle fuel consumption and emissions. The target speed of the SPD-HARM system is typically based on the occupancy of the target section. The desired speed limit is determined by a critical occupancy, control gains, and the previous speed limit (*21*). Typically, the TMC broadcasts the recommended target speed via connected vehicle communication and VSL signs.

In this scenario, the SPD-HARM section starts at milepost 51 on I-66 to the west and extends to milepost 60 on I-66 to the east. A recommended target speed of 87 km/h (54.4 mi/h) was utilized for the SPD-HARM section. Preliminary simulation tests were performed to find optimum target speed. Five target speeds (94, 87, 83, 78, and 73 km/h or 58.8, 54.4, 51.9, 48.8 and 45.6 mi/h) were compared and the target speed of 87 km/h (54.4 mi/h) was selected as the optimum speed for this specific network scenario. The target speed is almost identical to the mean value (86.9 km/h or 54.3 mi/h) of the speed-at-capacity at multiple locations in the study corridor. In this scenario, 100% of vehicles on the network are recommended to use the target speed.

The three-hour simulation was repeated 10 times with a different random seed in order to simulate multiple days. The simulation results, as illustrated in Figure 15, demonstrate that the proposed SPD-HARM system can reduce the system-wide total delay, fuel consumption, and emission levels compared with the base case scenario. In particular, the SPD-HARM system reduces total delay, fuel consumption, HC, CO, NO_x, and CO_2 emissions by 7.6%, 6.3%, 23.9%, 26.1%, 17.2%, and 4.4%, respectively, compared with the base case scenario. It is noted that the savings of HC, CO, and NO_x emissions for SPD-HARM operation are relatively greater than the typical emission reductions of the Eco-Lanes system. The low emission results of the SPD-HARM system are triggered by the relatively low average speeds of SPD-HARM vehicles compared with the Eco-Lanes applications.

Finally, the t-test results indicated that there were significant benefits to the MOEs when SPD-HARM was operated.

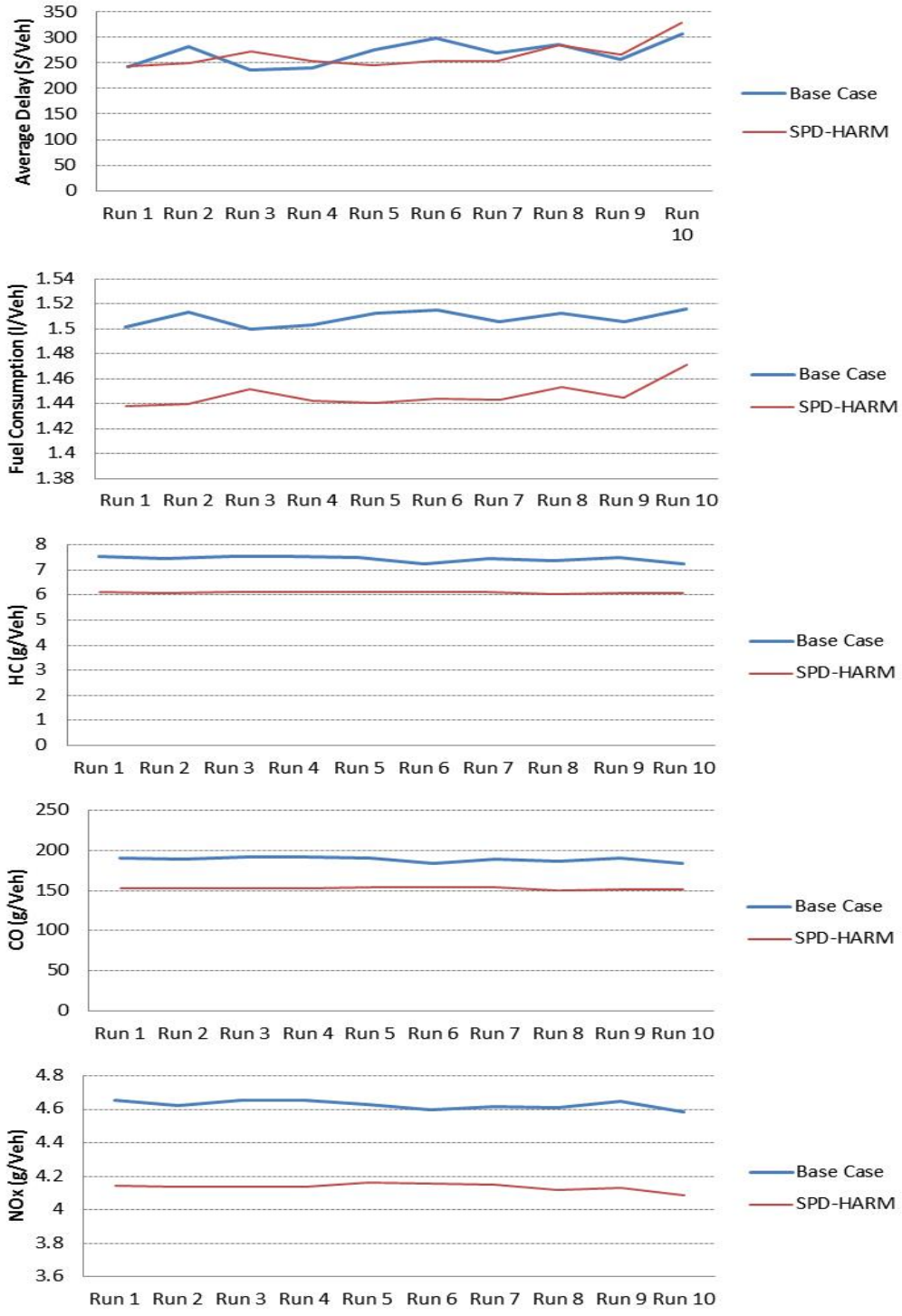

FIGURE 15: SPD-HARM results.

FINDINGS, CONCLUSIONS AND RECOMMENDATIONS

The study demonstrates the feasibility of two eco-driving applications which reduces vehicle fuel consumption and greenhouse gas emissions. The study develops an eco-drive system and Eco-Lanes applications. In particular, the study develops an eco-drive system that combines eco-cruise control logic with state-of-the-art car-following models and evaluates Eco-Lanes and SPD-HARM applications.

The research investigated the potential of developing an eco-drive system that combines an ECC system with state-of-the-art car-following models. The system makes use of topographic information, the spacing between the subject and lead vehicle, and a desired (or target) vehicle speed and distance headway as input variables. The study demonstrated that the proposed system can significantly improve fuel efficiency while maintaining reasonable vehicle spacing. One of the test vehicles, a 2011 Toyota Camry, saved 27 percent in fuel consumption with an average spacing of 47 m along the I-81 study section. The study found that the car-following threshold setting significantly affects the fuel economy and the spacing between vehicles. Furthermore, the study also demonstrated that a dynamic car-following spacing threshold significantly reduces the average vehicle spacing compared to a fixed car-following spacing threshold. The study also evaluated the impacts of variable vehicle power and found that vehicle operations at lower power demands significantly enhance vehicle fuel economy (up to 49 percent). The study finally demonstrated that non-ECC-equipped vehicles can significantly reduce their own fuel consumption just by following a lead ECC-equipped vehicle.

This research investigated the feasibility of Eco-Lanes applications that attempt to reduce system-wide fuel consumption and GHG emission levels through lane management strategies. The study focused its efforts on evaluating various Eco-Lanes and SPD-HARM applications using the INTEGRATION microscopic traffic simulation software. The study demonstrated that the proposed Eco-Lanes system can significantly improve fuel efficiency and air quality while reducing average vehicle travel time and total system delay. For this case study, the proposed system reduced travel time, delay, fuel consumption, HC, CO, and CO2 emissions by 8.5%, 23%, 4.5%, 3.1%, 3.4%, and 4.6%, respectively, compared with the base case scenario. The study also examined the feasibility of a predictive Eco-Lanes system. This system predicts the onset of congestion and starts the Eco-Lanes system before congestion occurs. The simulation study found that the 30-minute predictive Eco-Lanes system produced greater reductions in fuel consumption and CO2 emissions compared with the non-predictive Eco-Lanes system. The study also found that the optimum throttle levels and the optimum eco-speed limits can significantly improve the mobility, energy savings, and air quality of such systems. Furthermore, the study demonstrated that SPD-HARM as an Eco-Lanes application produced reductions in delay, fuel consumption, HC, CO, NOx, and CO2 emissions by 7.6%, 6.3%, 23.9%, 26.1%, 17.2%, and 4.4%, respectively, compared with the base case scenario.

Future research should quantify the potential benefits of using the proposed Eco-Lanes systems on different networks with various vehicle types. Also, further studies are required to characterize the optimum eco-lanes specifications, such as the spatial and temporal eco-lanes boundaries, and to enhance the optimum eco-speed limit algorithms.

Furthermore, the car-following behavior of non-eco-vehicles should be investigated. Finally, further research is needed to validate the simulation outputs using field tests.

REFERENCES

1. National Research Council (U.S.), *Expanding metropolitan highways : implications for air quality and energy use*. 1995, Washington, D.C.: Transportation Research Board. viii, 387.
2. Cicero-Fernandez, P., Long, J.R., and Winer, A.M., *Effects of grades and other loads on on-road emissions of hydrocarbons and carbon monoxide.* Journal of the Air & Waste Management Association, 1997. **47**(8): p. 898-904.
3. Park, S. and Rakha, H., *Energy and Environmental Impacts of Roadway Grades.* Transportation research record, 2006(1987): p. 13.
4. Boriboonsomsin, K. and Barth, M. *Fuel and CO2 Impacts from Advanced Navigation Systems that Account for Road Grade*. in *Presented at 88th Annual Meeting of the Transportation Research Board*. 2009. Washington, D.C.
5. Ahn, K., Rakha, H., and Moran, K. *Eco-Cruise Control Systems: Feasibility and initial Testing*. in *Presented at 90th Annual Meeting of the Transportation Research Board*. 2011. Washington, D.C.
6. Park, S., Rakha, H., Ahn, K., and Moran, K. *Predictive Eco-Cruise Control: Algorithm and Potential Benefits*. in *IEEE forum on integrated and sustainable transportations systems(FISTS)*. 2011. Vienna, Austria.
7. U.S. Department of Transportation. *AERIS TRANSFORMATIVE CONCEPTS*. 2011 [cited 2013 July 20th]; Available from: http://www.its.dot.gov/aeris/pdf/Draft_Transformative_Concepts.pdf.
8. U.S. Department of Transportation. *Applications for the Environment: Real-Time Information Synthesis (AERIS)* 2013 2013 July 30th]; Available from: http://www.its.dot.gov/aeris/.
9. U.S. Department of Transportation. *Dynamic Eco-lane Modeling*. 2013 [cited 2013 July 20th]; Available from: http://www.its.dot.gov/aeris/pdf/AERIS%202013%20Workshop%20--%20Dynamic%20Eco%20Lanes%20Modeling%20Handout%2003-18-2013.pdf.
10. U.S. Department of Transportation. *Dynamic Eco-Lanes Transformative Concept*. 2013 July 20th, 2013]; Available from: http://www.its.dot.gov/aeris/pdf/AERIS%202013%20Workshop%20--%20Dynamic%20Eco-Lanes%20ConOps%20Handout-03-14-2013.pdf.
11. Ploeg, J., Scheepers, B.T.M., van Nunen, E., van de Wouw, N., and Nijmeijer, H. *Design and Experimental Evaluation of Cooperative Adaptive Cruise Control*. in *14th International IEEE Conference on Intelligent Transportation Systems*. 2011. Washington D.C.
12. Shladover, S.E., *Literature Review on Recent International Activity in Cooperative Vehicle – Highway Automation Systems*, T. Office of Corporate Research, and Innovation Management, Editor 2012, Federal Highway Administration: Washington, DC. p. 25.
13. Shladover, S.E., *Recent International Activity in Cooperative Vehicle-Highway Automation Systems*, T. Office of Corporate Research, and Innovation Management, Editor 2012, Federal Highway Administration: Washington, DC. p. 81.

14. Shladover, S.E., Nowakowski, C., Cody, D., et al., *Effects of Cooperative Adaptive Cruise Control on Traffic Flow: Testing Drivers' Choices of Following Distances*, 2009, University of California, Berkeley: Richmond, CA. p. 98.
15. Nowakowski, C., O'Connell, J., Shladover, S.E., and Cody, D., *Cooperative Adaptive Cruise Control: Driver Acceptance of Following Gap Settings Less than One Second.* Proceedings of the Human Factors and Ergonomics Society Annual Meeting, 2010. **54**(24): p. 2033-2037.
16. Nowakowski, C., Shladover, S.E., Cody, D., et al., *Cooperative Adaptive Cruise Control: Testing Drivers' Choices of Following Distances*, 2011, California Partners for Advanced Transit and Highways. p. 142.
17. Park, B.B., Malakorn, K., and Lee, J., *Quantifying Benefits of Cooperative Adaptive Cruise. Control Toward Sustainable Transportation System*, 2011, University of Virginia.
18. Metz, N., Schlichter, H., and Schellenberg, H., *Positive effects of a traffic control system on fuel consumption and exhaust emission on the German A9 autobahn.* International Journal of Vehicle Design, 1997. **18**(3-4): p. 354-367.
19. Lee, C., Hellinga, B., and Saccomanno, F., *Evaluation of variable speed limits to improve traffic safety.* Transportation Research Part C-Emerging Technologies, 2006. **14**(3): p. 213-228.
20. Waller, S.T., Ng, M., Ferguson, E., Nezamuddin, N., and Sun, D., *Speed Harmonization and Peak-period Shoulder Use to Manage Urban Freeway Congestion* 2009, The University of Texas at Austin.
21. Kwon, E., Brannan, D., Shouman, K., Isackson, C., and Arseneau, B., *Development and field evaluation of variable advisory speed limit system for work zones.* Transportation Research Record, 2007(2015): p. 12-18.
22. Bertini, R.L., Boice, S., and Bogenberger, K., *Dynamics of variable speed limit system surrounding bottleneck on German autobahn.* Traffic Signal Systems and Regional Systems Management 2006, 2006(1978): p. 149-159.
23. Chang, G.L., Park, S.Y., and Paracha, J., *Intelligent Transportation System Field Demonstration Integration of Variable Speed Limit Control and Travel Time Estimation for a Recurrently Congested Highway.* Transportation Research Record, 2011(2243): p. 55-66.
24. Fudala, N.J. and Fontaine, M.D., *Interaction Between System Design and Operations of Variable Speed Limit Systems in Work Zones.* Transportation Research Record, 2010(2169): p. 1-10.
25. Kang, K.P., Chang, G.L., and Zou, N., *Optimal dynamic speed-limit control for highway work zone operations.* Maintenance Management and Services, 2004(1877): p. 77-84.
26. Lee, J., Dailey, D.J., Bared, J., and Park, B. *SIMULATION-BASED EVALUATIONS OF REAL-TIME VARIABLE SPEED LIMIT FOR FREEWAY RECURRING TRAFFIC CONGESTION* in *2013 Transportation Research Board* 2013. Washington D.C.
27. Rakha, H., Ahn, K., Moran, K., Saerens, B., and Bulck, E.V.d., *Virginia Tech Comprehensive Power-Based Fuel Consumption Model: Model development and*

testing Transportation research. Part D, Transport and environment, 2011. **16**(7): p. 492-503

28. Ni, D. and Henclewood, D., *Simple Engine Models for VII-Enabled In-Vehicle Applications.* IEEE Transactions on Vehicular Technology, 2008. **57**(5): p. 2695-2702.
29. Rakha, H., Ahn, K., Faris, W., and Moran, K. *Simple Vehicle Powertrain Model for use in Traffic Simulation Software*. in *Presented at 89th Annual Meeting of the Transportation Research Board*. 2010. Washington, D.C.
30. Van Aerde, M. *Single regime speed-flow-density relationship for congested and uncongested highways*. in *74th TRB Annual Conference*. 1995. Washington DC.
31. Van Aerde, M. and Rakha, H. *Multivariate calibration of single regime speed-flow-density relationships*. in *Proceedings of the 6th 1995 Vehicle Navigation and Information Systems Conference*. 1995. Seattle, WA, USA: Vehicle Navigation and Information Systems Conference (VNIS) 1995. IEEE, Piscataway, NJ, USA,95CH35776..
32. Rakha, H. and Arafeh, M., *Calibrating Steady-State Traffic Stream and Car-following Models using Loop Detector Data.* Transportation Science, 2009. **DOI: 10.1287/trsc.1090.0297**.
33. Rakha, H., *Validation of Van Aerde's Simplified Steady-state Car-following and Traffic Stream Model.* Transportation Letters: The International Journal of Transportation Research, 2009. **1(3)**: p. 227-244.
34. Rakha, H. and Lucic, I., *Variable power vehicle dynamics model for estimating maximum truck acceleration levels.* Journal of transportation engineering, 2002. **128**(5): p. 412-419.
35. Rakha, H., Snare, M., and Dion, F., *Vehicle dynamics model for estimating maximum light-duty vehicle acceleration levels.* Transportation Research Record, 2004. **n 1883**: p. 40-49.
36. Rakha, H., Lucic, I., Demarchi, S.H., Setti, J.R., and Van Aerde, M., *Vehicle dynamics model for predicting maximum truck acceleration levels.* Journal of Transportation Engineering, 2001. **127**(5): p. 418-425.
37. Park, S., Rakha, H., Ahn, K., and Moran, K., *Fuel Economy Impacts of Manual, Conventional Cruise Control, and Predictive Eco-Cruise Control Driving.* Accepted for Presentation at 92th Annual Meeting of the Transportation Research Board, Washington D.C., 2013.